Advancing cardiac safety and drug discovery screening using human stem cell-derived cardiomyocytes

Korte, T. de

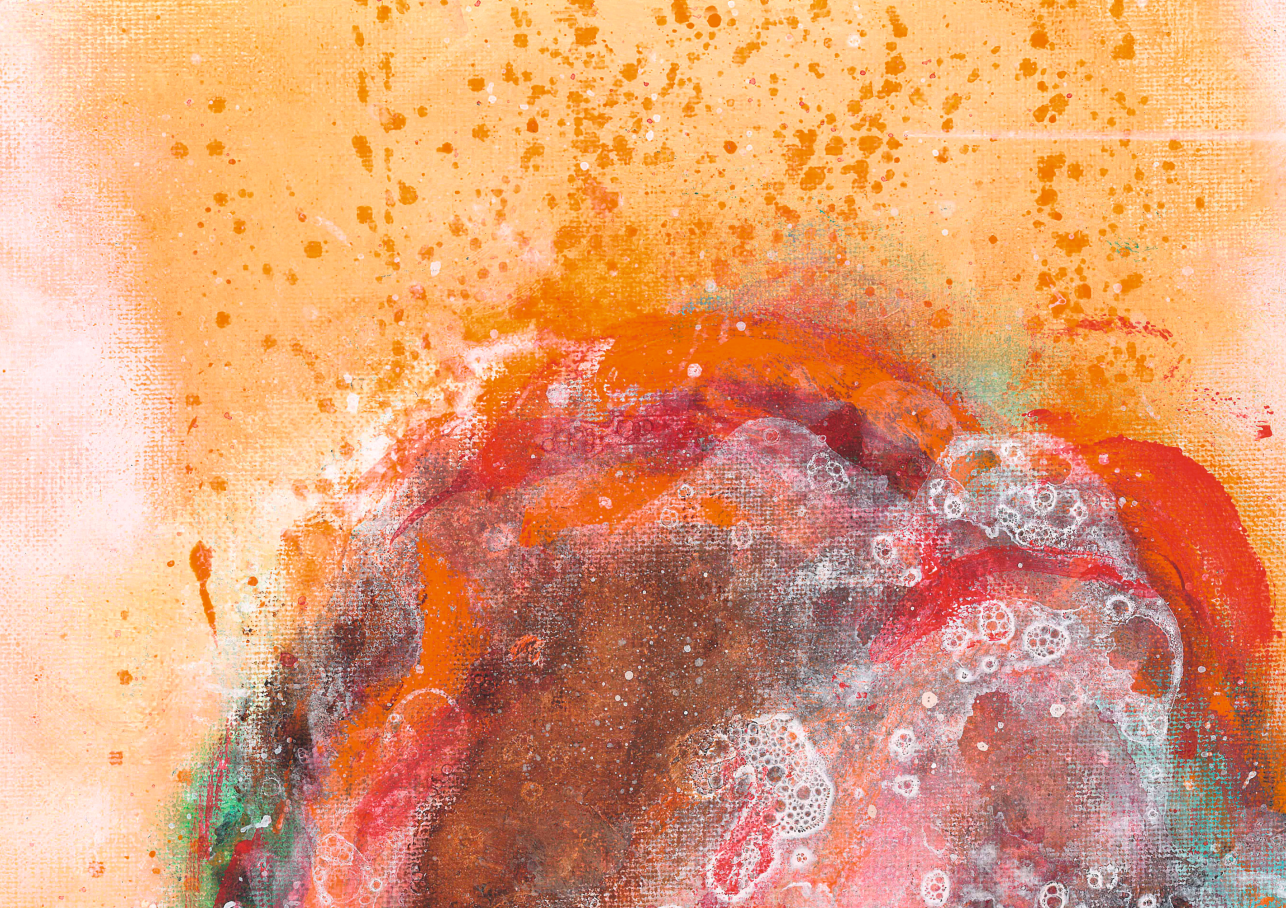

Novel studies conducting cardiac safety assessment using human-induced pluripotent stem cell-derived cardiomyocytes (hiPSC-CMs) are promising but might be limited by their specificity and predictivity. It is often challenging to correctly classify ion channel blockers or to sufficiently predict the risk for Torsade de Pointes (TdP). In this study, we developed a method combining *in vitro* and in silico experiments to improve machine learning approaches in delivering fast and reliable prediction of drug-induced ion-channel blockade and proarrhythmic behaviour. The algorithm is based on the construction of a dictionary and a greedy optimization, leading to the definition of optimal classifiers. Finally, we present a numerical tool that can accurately predict compound-induced pro-arrhythmic risk and involvement of sodium, calcium and potassium channels, based on hiPSC-CM field potential data.

5

A greedy classifier optimization strategy to assess ion channel blocking activity and proarrhythmia in hiPSC-cardiomyocytes

Fabien Raphel[1,2†], Tessa de Korte[3,4†], Damiano Lombardi[1],
Stefan Braam[3], Jean-Frederic Gerbeau[1]

[1] Inria, Paris, France,
[2] NOTOCORD part of Instem, Le Pecq, France,
[3] Ncardia, Leiden, Netherlands
[4] Department of Anatomy and Embryology, Leiden University Medical Centre, Leiden, The Netherlands
[†] These authors contributed equally to this work.

Published in PLoS Computational Biology. 2020;16(9):e1008203.

Author summary

Being able to measure the electrophysiology of human-induced pluripotent stem cell-derived cardiomyocytes (hiPSC-CMs) using multi-electrodes arrays (MEA) is promising in view of introducing novel drug screening methodologies in cardiac safety assessment in a preclinical setting. However, with new opportunities come new challenges. Data generated from hiPSC-CM MEA assays are challenging to interpret and translate to the clinical situation. Moreover, the observed experimental variability of the traces makes it difficult to assess whether we can systematically address classification problems such as channel blockade prediction, or arrhythmia risk. It would be of the utmost importance to understand if, in the Field potentials, there is enough information about these phenomena, and how it could be extracted. The method investigated is a first step towards this, and it is based on the construction of a dictionary of signal features: some of them are known markers used in electrophysiology, some are more agnostical signal characteristics. A goal oriented search is performed, in such a way that the input of the classifiers is found in order to maximise the success rate. Since, in general, the number of available experimental traces is not large enough to cover all the possible scenarios of interest, the experimental training set is complemented by an *in silico* training set. This method was applied to arrhythmic risk prediction on *in silico* data and channel blockade prediction on combined *in silico* and *in vitro* data. A conceptual scheme of the main points of the present contribution is presented in Figure1.

Introduction

The Comprehensive *in vitro* Proarrhythmia Assay (CiPA) is an initiative for a new paradigm in safety pharmacology to redefine the non-clinical evaluation of Torsade de Pointes (TdP)[1–3]. It aims to more precisely assess TdP risk *in vitro* by using a multifaceted approach that combines *in vitro* evaluations of electrophysiological responses in human-induced pluripotent stem cell-derived cardiomyocytes (hiPSC-CMs) and *in silico* models providing reconstructions of drug effects on ventricular electrical activity[4,5].

Since CiPA, *in vitro* studies using hiPSC-CMs become an increasingly integrated part of today's cardiac safety assessment. While encouraging, adequately predicting TdP risk of unknown drugs based on *in vitro* studies alone is challenging[6]. Besides, the analysis of the large data sets derived from those studies is often far from being automated.

One of the main challenges in proposing a high-throughput screening based on novel devices is often related to the variability of the signals measured, that could pose sensible questions about the ability to extract useful information from them. The main impact of the present work is related to this aspect, and the proposed framework can be considered as a first preliminary step towards the setup of a systematic procedure.

The main focus of the present study is to investigate a computational tool that combines statistical analysis and machine learning approaches (used in this context in[7]) to the mathematical modeling and the numerical simulations (*in silico* experiments) of the drug effects on the field potential (FP) of hiPSC-CMs obtained by multi-electrode array (MEA) technology.

Two problems of interest in the pharmacology community will be addressed: the first one is related to the prediction of the proarrhythmic behaviour of a drug, and the second one to the ion channels blockade (see Figure1 for a summary of the main key points of the article). These are typical classification tasks. Some classification studies in cardiac electrophysiology were proposed in the literature, on simulated action potentials[7,8] or ECG[9,10].

The contributions of the present paper are the following:

1. A dictionary based greedy optimisation method is proposed, that selects the most pertinent signal features to maximise the classification score. This procedure helps correct the classical markers used to analyse Field Potential signals and provides encouraging results.

2. The *in vitro* dataset is complemented by an *in silico* dataset. This makes it possible to explore all the possible scenarios and help mitigate the high-dimensional/low sample size regime potentially affecting the performances of the classifiers.

3. In constructing the signal database, the uncertainties affecting the experimental setup are accounted for. Despite many variability sources, the proposed approach aims at defining a robust classifier. Concerning the problems considered in the present manuscript, in the Field Potential there is enough information to provide an answer to them, irrespective of all the uncertainties affecting the experimental setup.

4. The proposed approach was tested on real data coming from actual experiments performed with MEA technology.

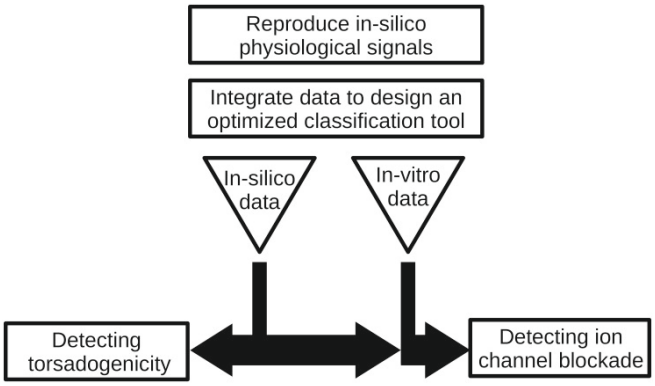

Figure 1. Summary of the main key points of the article.

The work is structured as follows: the first part is dedicated to the methods used to reproduce *in silico* physiological signals (FP and calcium transient signals) based on the bidomain equations[11] and the O'Hara, Virág, Varró and Rudy (ORd) ionic model[12]. The relation between drug concentration and ion channel activity is rendered through scaling factors depending on IC_{50} values (as proposed in[13–15]. The outputs of the *in silico* model are the simulations of the Field Potentials (FPs) recorded from extracellular micro electrodes, and the averaged calcium transient on a well ($[Ca^{2+}]_i$).

The second part is dedicated to the description of the method used to integrate *in silico* experiments and *in vitro* data in order to design an optimised classification tool. The proposed approach is based on the construction of a dictionary of linear and non-linear forms applied to the set of *in vitro* and *in silico* data; a greedy algorithm is defined to build a sparse observation-to-prediction relation.

Finally, we applied the classification process in two situations: detecting torsadogenicity (TdP risk versus non-TdP risk) with a synthetic dataset and detecting ion channel blockade (for sodium, calcium or potassium channels) by the action of a given compound, on *in vitro* MEA data.

The classification results obtained show that the double greedy optimization strategy is effective in improving classifiers performances (with only a few parameters to be tuned) and is well adapted to study compound effects on hiPSC-CM electrophysiology that will aid in early and predictive cardiac safety assessment.

Materials and methods

In this section, we present the method developed to improve the classification of electrophysiological regimes based on MEA signals. It consists in fusing together information coming from available experimental MEA data and numerical simulations in order to design the classifiers to be used.

First, the experimental methods are described; then, we show the different models used to reproduce FPs and calcium signals (MEA computational model) and we end the section by presenting the optimised classification algorithm (Classification) and the definition of the dictionary entries (Dictionary construction). The structure of this section is shown in Figure2.

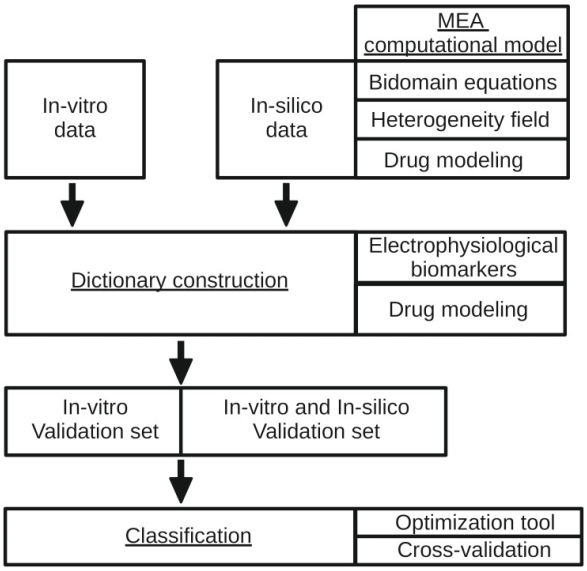

Figure 2. Scheme of the materials and methods section.

Experimental setup

The methods used to perform the experiments and acquire the recordings of the FPs are presented in detail below.

Cell culture

Human iPSC-CMs (Pluricyte® Cardiomyocytes, Ncardia, Leiden, The Netherlands) were stored in liquid nitrogen until thawed and cultured onto 96 well MEA plates (Axion Biosystems, Inc., Atlanta, USA) according to manufacturer instructions. Briefly, the MEA plates were coated with fibronectin (50μg/ml in PBS [+ Ca^{2+} and Mg^{2+}], Sigma-Aldrich, St. Louis, MO, USA; Cat. No. F-1141) for 3 hours at 37°C and 5% CO2. After 3 hours of incubation time, the excess of fibronectin coating solution was removed and cells were plated in a 5 μl droplet at a density of 25,000 cells/well. After 1 hour of incubation (37°C and 5% CO2), 100 μl pre-warmed (37°C) medium (Pluricyte® Cardiomyocyte Medium, Ncardia, Leiden, The Netherlands) was carefully added to each well. Cells were maintained in Pluricyte® Cardiomyocyte Medium for 8 days and refreshments took place at day 1 post-thaw and subsequently every other day. MEA recordings were performed at day 8 post-thaw. The choice of these different parameters of the experimental setup was presented and commented in[16].

Test compounds

At day 8 post-thaw, medium was refreshed at least 2 hours before compound addition. The 12 test compounds were provided by the Chemotherapeutic Agents Repository of the National Cancer Institute and consisted of a random subset of CiPA compounds. The compounds were from 3 clinical TdP risk categories: low/no (Loratadine, Mexiletine, Diltiazem), intermediate (Clozapine, Chlorpromazine, Clarithromycine, Cisapride, Droperidol) and high (Ibutilide, Dofetilide, Bepridil, Azimilide)[17] (see Table 1). Chemical stock solutions at 1000 folds of the target concentrations were prepared under sterile conditions in DMSO and stored at –20°C, according to HESI Myocyte Phase II Validation Study Protocol instructions. The serial diluted compounds were further prepared in DMSO on the day of compound assay. The 10–fold final dilutions of the compounds were prepared with Pluricyte® Cardiomyocyte Medium, for single time use only. Pluricyte® Cardiomyocytes were exposed to four different concentrations of the compound, under sterile conditions in single point additions (i.e. one concentration per well) in five replicates for each concentration. Vehicle control was 0.1% DMSO.

Ethic statement

All the experiments were performed under permits granted from the Commissie Medische Ethiek Leiden University Medical Center (permit number: NL45478.058.13).

Table 1. Experimental data information. IC_{50}, Concentrations and C_{max} are given in μM. T/V column corresponds to the compound embedding into the Training set (T) or Validation set (V).

Compound*	IC50**			Concentration				C_{max}***	T/V	Label
	hERG	Cav1.2	Nav1.5	#1	#2	#3	#4			
Loratadine	6.1	11.4	28.9	0.001	0.003	0.0095	0.03	0.00046	V	K [39], Ca [40]
Ibutilide	0.018	62.5	42.5	0.0001	0.001	0.01	0.1	0.1	T	K [41]
Droperidol	0.06	7.6	22.7	0.03169	0.10014	0.31646	1.0	0.02	T	K [41]
Mexiletine	62.2	125	38	0.1	1.0	10	100	2.5	T	Na [42], K [43]
Dofetilide	0.03	26.7	162.1	0.0003	0.001	0.0032	0.01	0.002	V	K [41]
Diltiazem	13.2	0.76	22.4	0.01	0.1	1.0	10	0.13	T	Ca [44]
Chlorpromazine	1.5	3.4	3.0	0.0951	0.3004	0.9494	3	0.0345	V	K [41], Ca [45], Na [46]
Clozapine	2.3	3.6	15.1	0.0951	0.3004	0.9494	3	0.07	T	K [47], Ca [40]
Clarithromycine	32.9	>30	NA	0.1	1	10	100	1.2	V	K [41]
Cisapride	0.02	11.8	337	0.0032	0.01	0.0316	0.1	0.0026	V	K [41]
Bepridil	0.16	1.0	2.3	0.01	0.1	1	10	0.03	V	K [41], Ca [48], Na [48]
Azimilide	<1†	17.8†	19†	0.01	0.1	1	10	0.07	V	K [49], Na [50], Ca [50]

* TdP risk (low, medium or high) Colatsky *et al* [17].

** From Ando *et al* [51].

*** From Blinova *et al* [6].

† From Yao *et al* [50].

MEA recordings

At day 8 post-thaw, 96 well MEA plates seeded with hiPSC-CMs were placed in the Maestro MEA device (768-channel amplifier) with an integrated heating system, temperature controller and data acquisition interface (Axion BioSystems, Inc., Atlanta, USA). The field potential traces of the hiPSC-CMs were recorded prior to (baseline) and 30 min after compound addition for 5 min. The recording conditions were at 37°C using Cardiac Standard filters and amplifiers in spontaneous cardiac mode (12.5 Hz sampling frequency, 2 kHz Kaiser Window, 0.1 Hz IIR). The beat detection threshold was 300 μV.

MEA computational model

This part provides a detailed description of the mathematical models used to simulate FPs in a realistic MEA geometry. Simulated FP studies were already performed for *in silico* assessment of drugs effects[14] or channel activity identification[18] and have shown the potency to reproduce and analyze compound effects on cardiac electrophysiology.

The first section concerns the bidomain equations, which governs the electrical activity propagation in a tissue. Since in a well the cells might not be perfectly uniformly distributed and the cell population might even be heterogeneous, a stochastic model of the population distribution was adopted, which is described in section Heterogeneity. In the last part

(Drug modeling) we describe the compound simulation strategy, aiming at reproducing the experimental protocol used to classify reference compounds holding ion channel blocking properties.

Bidomain equations

To simulate MEA recordings, the bidomain Eq[1] were solved on a domain $\mathcal{D}$, representing a well, by using a finite element method. The main geometrical hypothesis is that the cardiac cells in the well form a monolayer; therefore, to write the model, it is reasonable to consider a two dimensional domain, $D \subset \mathbb{R}^2$.

The equations read:

$$\begin{cases} A_{\mathrm{m}} C_{\mathrm{m}} \dfrac{\partial V_{\mathrm{m}}}{\partial t} + A_{\mathrm{m}} I_{\mathrm{ion}}(V_m, w) - \nabla \cdot (\sigma_{\mathrm{i}} \nabla V_{\mathrm{m}}) - \nabla \cdot (\sigma_{\mathrm{i}} \nabla \phi_{\mathrm{e}}) = A_{\mathrm{m}} I_{\mathrm{app}}, \\ -\nabla \cdot ((\sigma_{\mathrm{i}} + \sigma_{\mathrm{e}}) \nabla \phi_{\mathrm{e}}) - \nabla \cdot (\sigma_{\mathrm{i}} \nabla V_{\mathrm{m}}) = \dfrac{1}{z_{\mathrm{thick}}} \displaystyle\sum_{e_k} \frac{I_{\mathrm{el}}^k}{|e_k|} \chi_{e_k}, \end{cases} \tag{1}$$

where A_{m} is the surface area of the membrane per unit volume of tissue, C_{m} the membrane capacitance and z_{thick} the thickness of the cell layer. V_{m} and $\boldsymbol{\phi}_e$ correspond respectively to the transmembrane potential and extracellular potential and I_{ion} is the ionic model depending on V_{m} and the gating variables. The propagation velocity is carried by the intracellular and extracellular conductivity ($\boldsymbol{\sigma}_i$ and $\boldsymbol{\sigma}_e$ respectively). The boundary conditions used with the bidomain equations are the following: $\boldsymbol{\sigma}_{\mathrm{i}} \nabla \boldsymbol{\phi}_{\mathrm{i}} \cdot \mathrm{n} = 0$ (with $\boldsymbol{\phi}_i = V_m + \boldsymbol{\phi}_e$), and either $\boldsymbol{\phi}_e = 0$ on the region connected to the electrical ground or $\boldsymbol{\sigma}_{\mathrm{e}} \nabla \boldsymbol{\phi}_e \cdot \mathrm{n} = 0$ elsewhere.

To take the impact of the electrodes on the signal into account, an imperfect electrode model[18] is coupled to the bidomain equations. The model is described in Eq 2.

$$\frac{dI_{el}^k}{dt} + \frac{I_{el}^k}{\tau} = \frac{C_{el}}{\tau} \frac{\phi_{e,mean}^k}{dt}, \tag{2}$$

where $\boldsymbol{\phi}^k_{e,mean}$ is the averaged extracellular potential on the electrode e_k, R_{el} and C_{el} are the electrode resistance and electrode capacitance respectively and R_i is the internal resistance of the measurement device. $\tau = C_{el}(R_i + R_{el})$ is the time constant of the RC circuit. Then, the field potential $\boldsymbol{\phi}^k_f$ measured on the electrode e_k is given by $\boldsymbol{\phi}^k_f = R_i I^k_{el}$. For this study, electrodes parameters values used are summarized in Supplementary Table A.

The ionic current $I_{\mathrm{ion}}(V_m, w)$ and the state variable w are provided by the ORd model[12]. Three types of cells are considered to mimic the monolayer heterogeneity (Heterogeneity):

Epicardial, Mid-myocardial and Endocardial. These cell types are simulated through specific sets of parameters given in[12]. This model takes into account the main concentration dynamics ($[Na^+]_i$, $[Ca^{2+}]_i$ and $[K^+]_i$). The current $I_{app} = I_{app}(x, y, t)$ is the origin of the activation. The source is supposed to be located in a unique region and is defined as follows:

$$I_{\text{app}}(x, y, t) = \begin{cases} I_0 \exp\left[\frac{(t-t_0)^2}{2\sigma^2}\right] & \text{if } (x - x_0)^2 + (y - y_0)^2 \leq r^2, \\ 0, & \text{otherwise,} \end{cases} \tag{3}$$

where the position (x_0, y_0) is drawn randomly and $r = 50\ \mu m$ is the radius of the source. $I_0 = -130 pA/pF$ is the maximum stimulation value, t_0 is the time when I_{app} is at its maximum and $\sigma = \Delta t/6$ with $\Delta t = 4$ ms.

The discretization of the partial differential equation was done in space using P1 Lagrangian finite elements and in time using backward differentiation formula (BDF) schemes with a time step of 0.1 ms. The ODE system governing the action potential modeling ($I_{ion}(V_m, \omega)$ in Eq 1) was solved using BDF scheme with adaptive time steps and order, whose implementation is provided by Sundials' CVODE[19]. These space and time discretizations of the bidomain equations were already used in different studies (*in silico* ECG and *in silico* field potentials) and have shown qualitatively good results compared with real data[14,18,20–23].

To mimic experimental measurements, a 10 μV standard deviation noise of a zero-mean Gaussian was added to FPs. As some devices are able to get the intracellular calcium transient by fluorescence, we made the assumption that we have access to intracellular calcium transient data. We added a zero-mean Gaussian noise of 10^{-3} μM on the intracellular calcium transient obtained by simulation with the ORd model.

Heterogeneity

The hiPSC-CMs used in this study are > 70% pure cardiomyocytes based on positive Troponin T (TnT) expression. At least 70% of the TnT positive cells express a ventricular phenotype (based on ventricular myosin light chain 2 (MLC2v) expression and patch clamp technology). The other 30% of the cell population are of mesodermal origin. The actual distribution of these cells inside the well is unknown, and is a source of uncertainty that we need to take into account when developing the classifier in order to provide meaningful results in realistic applications.

To simulate this heterogeneity in the cell distribution inside a well, a space stochastic process was introduced, similarly to what was proposed in[24]: let $(Z, \mathcal{A}, \mathcal{P})$ be a complete probability space, Z being the set of outcomes, $\mathcal{A}$ a σ–algebra and $\mathcal{P}$ a probability measure:

$$c(x, \zeta) : \Omega \times Z \rightarrow [0, 1]. \tag{4}$$

An hypothesis on the correlation of the process was made and expressed in Eq 5:

$$f_c\left[\begin{pmatrix} x \\ y \end{pmatrix}, \begin{pmatrix} x' \\ y' \end{pmatrix}\right] = \exp\left[-\frac{(x-x')^2 + (y-y')^2}{2l_c^2}\right], \tag{5}$$

that is, the correlation is normal and its length l_c was set to 0.25 mm, which corresponds approximately to the distance between two electrodes. A Karhunen-Loève expansion based on the diagonalisation of the correlation kernel was used in order to generate the heterogeneity fields (see[24] for details). As shown in[25] in a case of a low value for l_c, the medium is homogenised which leads to a decrease of the repolarization phase. The parameter l_c = 0.25 mm was a good choice to qualitatively reproduce FP signals and more precisely the repolarization phase.

When discretised on the finite element space (P1 Lagrangian elements were used), a cell type was affected to each node of the finite element mesh according to the following rule:

$$\text{CellType}_i = \begin{cases} \text{Epicardial, if } c_i < \frac{1}{3}. \\ \text{Mid} - \text{myocardial, if } c_i > \frac{2}{3}. \\ \text{Endocardial, otherwise.} \end{cases} \tag{6}$$

where $c_i \in^{0,1}$ is given by the random process c discretised at the node whose coordinates are $x^{(i)}$ (see Eqs 4 and 5). Example of random heterogeneity obtained with this method is presented in Figure3.

Drug modeling

In this study we assume that a drug may affect only sodium, calcium and/or potassium channels. If the properties of a compound are known (e.g., IC_{50} for each ionic channel) then the conductance-block model[13–15] can be used to render its action on the ion channels. This model rewritten in Eq (7) qualitatively reproduces the expected compound effect on FPs[20]:

$$g_s = g_{control,s}\left[1 + \left(\frac{[D]}{IC50_s}\right)^n\right]^{-1}, \tag{7}$$

where $g_{control,s}$ is the conductance of the channel s at control case (baseline), $[D]$ is the concentration of the drug and $IC50_s$ is the constant of the drug concentration at which current of channel s is blocked at 50%. We chose to set the Hill coefficient n at 1. The first reason is due to the confidence intervals of computed Hill coefficients for different compounds[26] which most of the time includes 1. The second reason comes from the use of the EFTPC in

our simulations. Varying the Hill coefficient between 0.6 to 1.4, the standard deviation of the channel activity is lower than 0.05 for concentrations higher than the IC_{50} and lower than 0.03 for concentrations lower than the IC_{50} (see Figure4). The use of the EFTPC leads to a low variability in the channel activity according to the Hill coefficient and studied compounds.

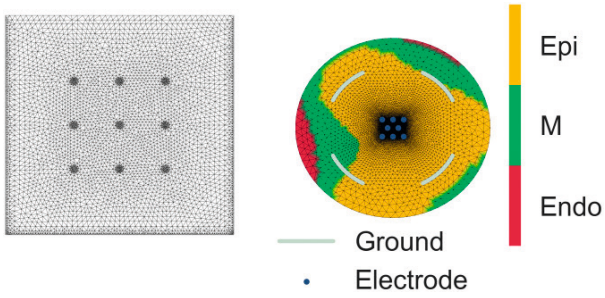

Figure 3. Finite element meshes of MEA used, and example of heterogeneity field. *Left: Finite element mesh representing one well including 9 electrodes of the 6–well MEA device from Multichannel Systems (used in TdP classification). Right: Finite element mesh representing one well including 8 electrodes of the 96–well MEA device from Axion Biosystems with an example of generated cell heterogeneity field (used in Channel classification).*

On the other hand, we can simulate unknown compounds, blocking randomly sodium, calcium and/or potassium channels. Figure5 shows an example of simulated early afterdepolarization (EAD) as a result of blocking IK_r current at 93.5%. The FP and intracellular calcium transient shapes are in good qualitative agreement with experimental signals[27,28].

Dictionary construction

In this section the details about the construction of the dictionary entries are provided and commented. As mentioned previously, the dictionary is a collection of linear and non-linear forms applied to the signals, corresponding to the definition of features (think, for instance, to the maximum of the signal, or its average, and so on). Since a greedy optimization strategy has been devised, and since the internal stages of the descent are easily parallelizable, the affordable dictionary size is potentially large (a few hundred in the study, potentially few thousands). In the present work, the dictionary is divided into two parts:

- non-agnostic, or informed.
- agnostic

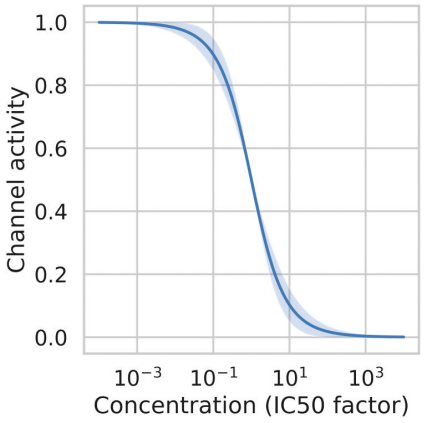

Figure 4. Channel activity average and standard deviation for a Hill coefficient varying from 0.6 to 1.4. *The abscisse is the concentration factor with respect to the* IC_{50}.

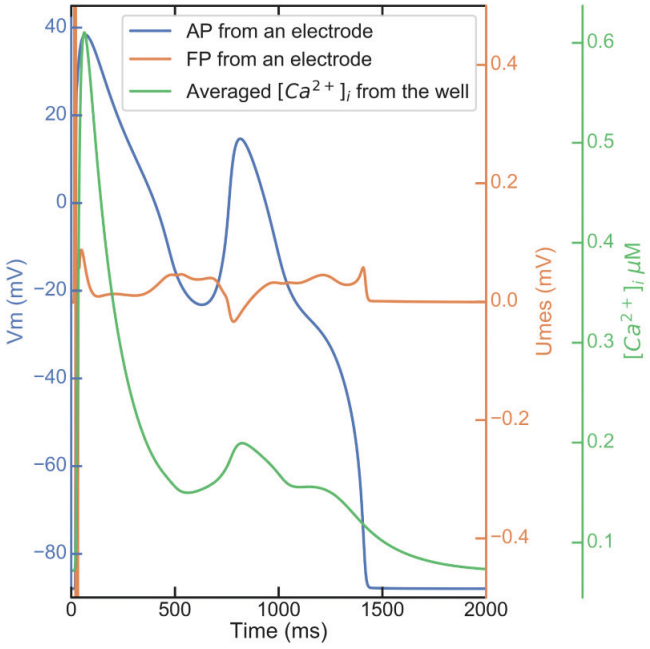

Figure 5. EAD simulation. *Transmembrane action potential (AP, blue), extracellular field potential (FP, orange) and intracellular calcium transient trace (green) in a simulated EAD case.*

In the informed part we collect the biomarkers extracted from the signal, identified by the experts as correlated to some regime of interest. These quantities are meant to reveal a particular state of the system or alteration of a parameter. For instance, altering the sodium channel activity induces a modification in the depolarization amplitude[29].

The second part of the dictionary is agnostic, meaning that the linear and non-linear forms introduced are extracted from the signal as a mathematical object. The goal of the agnostic part of the dictionary is to enrich it, henceforth increasing the possibilities of computing from the dictionary an input leading to a good classification. The dictionary entries and their numbering are presented in Supplementary Table D.

Dictionary entries: Electrophysiological biomarkers

First, some intuitive biomarkers were extracted, *e.g.* depolarization amplitude (DA), field potential duration (FPD), etc. These quantities (called parameters in the electrophysiology community) are presented in Figure 6.

Remark: In the electrophysiology community we often refer to parameters to designate quantities extracted from the experimental signals. In the present work, we follow the usage in applied mathematics and engineering communities, that name parameters the quantities affecting the state of the system and not the quantities read from the system observable. Their computation follows the work in[24] and it is described in more details in the supplementary material, section Field Potential Biomarkers computation. Concerning the calcium transient signal computation, details are given in the supplementary material, section Calcium Signals Biomarkers computation. As these values of these biomarkers are computed in control and drug case, we decided to use relative values to the control case. For instance, the DA ratio is: *DAdrug/DActrl*. The justification of this choice is shown in Figure 7. As we can see, even if the control case is different, the impact due to a compound is qualitatively the same regardless of the heterogeneity field.

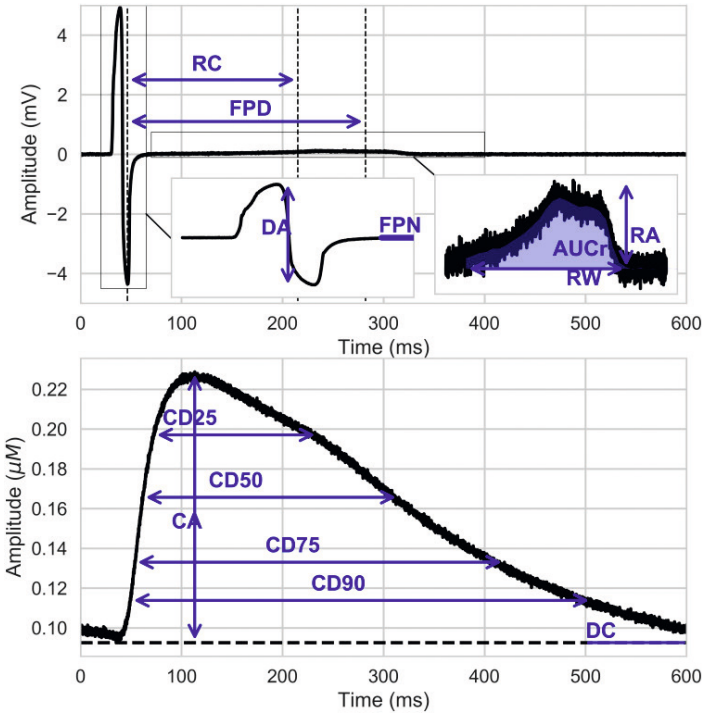

Figure 6. List of the parameters computed on FP (up) and Calcium transient (down). *RC: Repolarization Center; FPD: Field Potential Duration; DA: Depolarization Amplitude; FPN: Field Potential Notch; AUCr: Area Under Curve of the repolarization wave; RA: Repolarization Amplitude; RW: Repolarization Width; CA: Calcium Amplitude; DC: 'Drowsing Calcium'; CDX: Calcium Duration. See Sections Field Potential Biomarkers computation and Calcium Signals Biomarkers computation in the supplementary material.*

An example of an effect of a drug on the repolarization of the cells compared to baseline is presented in Figure 8. In a case where a drug does not affect the repolarization, we should obtain a curve similar to $f(x) = x$ (red line in Figure8). In the case where the repolarization is affected by a compound, a distortion appears on the signal (see black dots lower panel in Figure 8 corresponding to an increase in the FPD). Five markers (from K1 to K5) were extracted from the signal, with FP^{drug}_{rep} and FP^{ctrl}_{rep} the repolarization part of the FP for the drug and control case:

- Maximum distance: $max_i \sqrt{(FP^{drug}_{rep}(i) - FP^{ctrl}_{rep}(i))^2}$.
- ℓ^2 norm: $||FP^{drug}_{rep} - FP^{ctrl}_{rep}||_{\ell^2}$.
- Average deviation: $\frac{1}{N}\sum_{i=1}^{N}\left(FP^{drug}_{rep}(i) - FP^{ctrl}_{rep}(i)\right)$.
- Maximum deviation: $max_i(FP^{drug}_{rep}(i) - FP^{ctrl}_{rep}(i))$.
- Time of the maximum deviation.

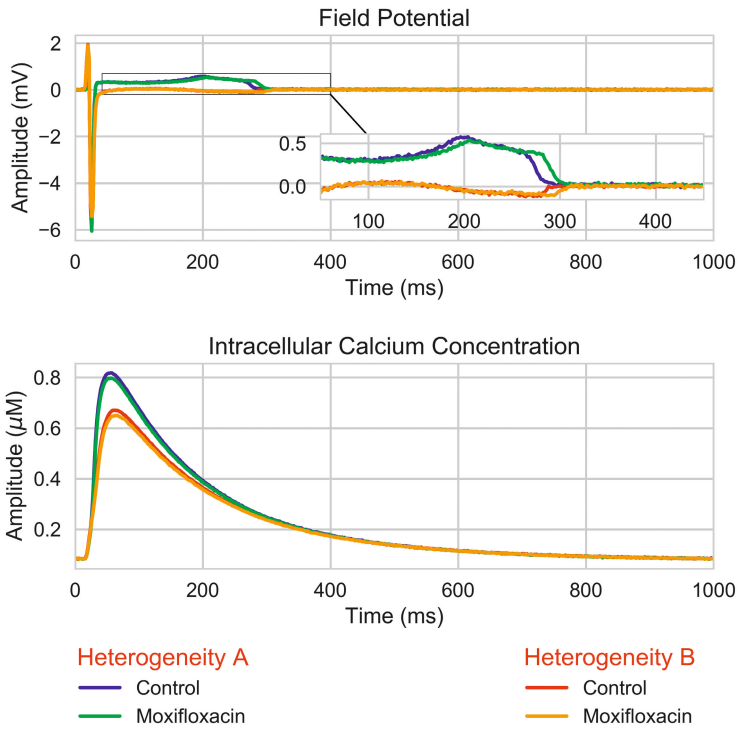

Figure 7. Electrophysiological biomarkers: Moxifloxacin simulation. *Simulation of the effect of Moxifloxacin at effective free therapeutic plasma concentration (10.96 μM, see Table F in the supplementary material) on the FP (from one electrode) and intracellular calcium transient (from one well) for two different heterogeneity fields. A finite element mesh of 96-well MEA device from Axion Biosystems was used for this simulation (see right panel of Figure3).*

Dictionary entries: Wavelets

In order to construct the agnostic part of the signal, a wavelet decomposition was considered for the repolarization phase. The number of coefficients retained is such that the signal could be represented up to the noise level by the wavelets expansion. When a new signal is analyzed, only the selected coefficients (already computed for the training database) are then used to reconstruct the signal. If the L^2 error is lower than an arbitrary value, we store these coefficients. Otherwise, we compute the new location and add the missing locations. The wavelet transform was done on the absolute difference between the drug case and the control case. An example of reconstruction is shown in Figure9. The algorithm to get the positions is presented in the pseudo-code 1.

Algorithm 1 Section Dictionary entries: wavelets: Wavelet coefficient.

1: N_s ▷ Number of signals to compute positions.
2: *thr* ▷ Threshold for the wavelets transform.
3: v_p ▷ Empty array of positions.
4: **for** $i \coloneqq 1$ **to** N_s **do**
5: f_i ▷ Get the i^{th} signal.
6: $c_{wvlt} = CWT(f_i, thr)$ ▷ Computes wavelets coefficients.
7: $v^{nz}{}_p$ ▷ Get the non-zeros positions of c_{wvlt}.
8: **if** i==1 **then**
9: $v_p = v^{nz}{}_p$
10: **else**
11: $v_p = v_p \cup v^{nz}{}_p$
12: **end if**
13: **end for**

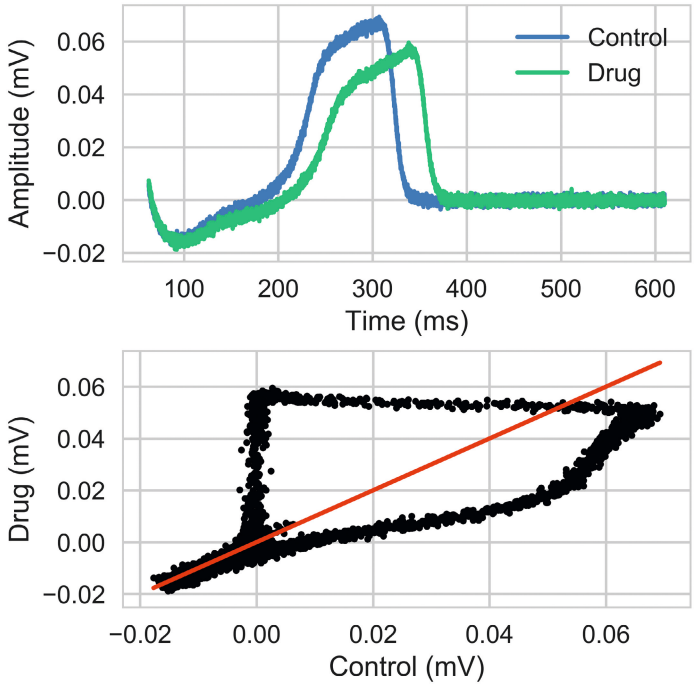

Figure 8. Electrophysiological biomarkers: Extended dictionary based on repolarization. *Upper panel: FP repolarization. Lower panel: Repolarization of cells affected by a compound with respect to the control case repolarization. The red line corresponds to the case where the repolarization is not affected.*

Classification

Given a molecule which is a candidate to become a drug, several questions arise concerning its impact on the electrical activity of cells. Basic questions like: *Is this drug blocking channel X?* or: *Is the drug potentially causing arrhythmia?* are naturally treated by solving a classification problem.

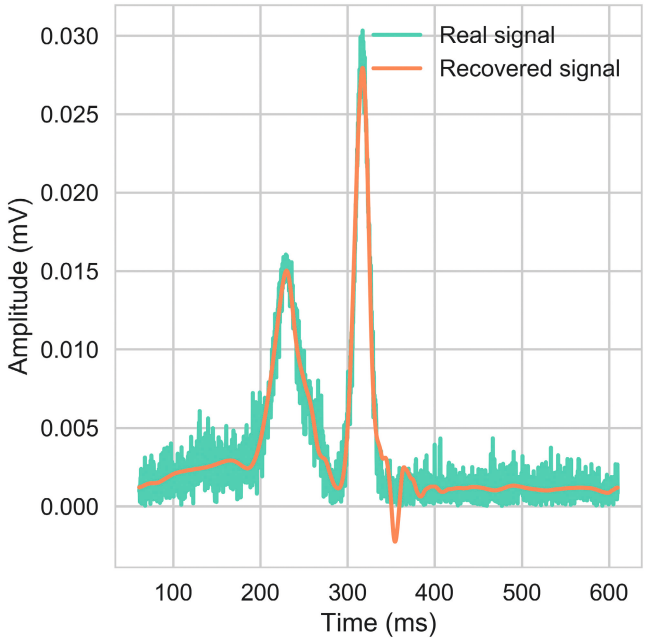

Figure 9. Wavelets: Signal reconstruction from wavelet coefficients. *Reconstruction of the absolute difference between the drug and control signals for the plateau and repolarization phases, based on wavelets coefficients.*

One of the main difficulties related to such a study is the curse of dimensionality[30] since we are dealing with high dimension, low sample size data. Otherwise stated, the function to be identified in view of setting up efficient classifiers is defined over a high dimensional domain and the number of available data is too low. To tackle this problem, numerical simulations were exploited. The rationale behind the strategy is twofold: first, we added virtual *in silico* experiments to the data set to increase the population size. Second, we exploited the simulations to extract meaningful low dimensional subsets of the data, which contributed to the mitigation of the high-dimensionality. Several methods are available in the literature to extract these low dimensional subsets[31].

However, the risk in using generic problem independent methods is that the subsets obtained could drastically reduce the amount of information conveyed about the quantity of interest to be classified. Henceforth, we constructed a low dimensional subset of the data that has been exploited in the classifier construction, designed to deliver optimal classification performances.

This method can be applied to all different classification techniques, and the result is classifier dependent.

Classification optimization

As stated, the aim was to set up a dimension reduction strategy in such a way that, when the extracted subset of the data is used as input for the classifier, we obtain optimal performances. The procedure reminds, in the spirit, the feature selection algorithms (and feature hashing), with some important differences, which will be highlighted later on.

First of all, for a classification problem, we needed to define a database of signal samples. Let $i \in \mathbb{N}^*, i \leq N_s$, the i-th signal sample is $z^{(i)}(t): \mathbb{R}^+ \rightarrow \mathbb{R}^m$, where m depends on the number of electrodes of the device, as well as the ability for instance to read intracellular calcium transients. The database contains either real signals coming from MEA experiments or numerical signals.

After having collected a database of N_s signals, we defined a dictionary of linear and non-linear forms that has been applied to the signal. Let $B_i = (b^i_1, \ldots b^i_{Nb})$ be the dictionary entries (features extracted from signals) of the i^{th} sample:

$$b_j^{(i)}(z^{(i)}) : \mathbb{R}^m \rightarrow \mathbb{R}. \tag{8}$$

The whole dictionary applied to the signals population is stored in a matrix $F_s \in \mathbb{R}^{Ns \times Nb}$. The input of the classifier is defined as a linear combination of the dictionary entries applied to a signal:

$$x \in \mathbb{R}^d, \tag{9}$$

$$x_k = \sum_{j=1}^{N_b} \omega_{kj} b_j(z), \quad k = 1, \ldots, d. \tag{10}$$

The weights ω_{kj} of the linear combination are stored in a matrix $\Omega \in \mathbb{R}^{d \times Nb}$. The goal, is to find the weights matrix which defines the input space maximizing the classification score, for a given classification strategy. The problem is recast as a minimization of a cost function, describing the classification performances.

In the binary classification case, let N_s be the number of samples, $l_i = \{-1, 1\}$ the true label of the i^{th} sample and $\hat{l}_i = \{-1,1\}$ the predicted label of the i^{th} sample associated with $\hat{P}_i \in [1/2,1]$ the confidence of the classifier to be the predicted label. n_1 (respectively n_{-1}) is the number of samples labeled as 1 (respectively -1) and is introduced to avoid a possible bias due to unbalanced classes. Then, we have $n_1 + n_{-1} = N_s$. The $\delta_i(x)$ function is the Dirac function ($\delta_k(x) = 1$

if $x = k$, 0 otherwise). Finally parameter $\alpha \geq 1$ is introduced to penalize the false positive case ($l_i = 1$ and $\hat{l}_i = -1$). The expression of the cost function is presented in Eq 11.

$$s_{N_s} = -\frac{1}{N_s}\sum_{i=1}^{N_s}\hat{p}_i\left[\frac{N_s}{n_1}\delta_1(\hat{l}_i)\delta_1(l_i) + \frac{N_s}{n_{-1}}\delta_{-1}(\hat{l}_i)\delta_{-1}(l_i) - \alpha\frac{N_s}{n_1}\delta_{-1}(\hat{l}_i)\delta_1(l_i) - \frac{N_s}{n_{-1}}\delta_1(\hat{l}_i)\delta_{-1}(l_i)\right]. \quad (11)$$

With this formulation, the minimum value of s_{Ns} is -2 and the highest value is $1 + \alpha$. See the demonstration in Cost function demonstration: 2 classes (supplementary material). The rationale of including the terms $\hat{P}_i$ in the cost function is to better describe the performances of the classifier, accounting for the confidence in the classification, and not merely on the success rate. This aims at setting up a robust classification tool. Following the same principles, the cost function can be extended to k classes as shown in Eq 12:

$$s_{N_s} = -\frac{1}{N_s}\sum_{i=1}^{N_s}\hat{p}_i\left\{\sum_{j=1}^{k}\left[\frac{N_s}{n_j}\delta_j(\hat{l}_i)\delta_j(l_i) - \frac{N_s}{n_j}\alpha_j\sum_{\substack{m=1\\m\neq j}}^{k}\delta_m(\hat{l}_i)\delta_j(l_i)\right]\right\}, \quad (12)$$

where n_j is the number of samples labeled j and $\alpha_j > 0$ the weight assigned if the predicted label is not the class j. The value obtained for the best case is $-k$ whereas the cost obtained in the worst case is $\sum_{j=1}^{k}\alpha_j$. Demonstrations are presented in Cost function demonstration: general case (supplementary material). In the case where we do not penalize classes, all the α_j are equal to 1.

A regularization term was added to the cost function:

$$s_{N_s,reg} = s_{N_s} + \beta\left(\sum_{k=1}^{d}(1 - \sum_{i=1}^{N_b}\omega_{ki}^2)\right), \quad (13)$$

where $\beta \in \mathbb{R}^+$ is a penalization parameter. This term aims at breaking the scaling invariance of the linear combination of the dictionary entries. In particular, if a linear classifier is used, let $\alpha \in \mathbb{R}$, $\alpha \neq 0$, the classification score when using $\alpha\,\Omega$ is the same as Ω, irrespective of the value of α.

The optimization problem reads:

$$\mathbf{\Omega}^* = \arg\inf_{\Omega\in\mathbb{R}^{d\times N_b}} s_{N_s,reg}. \quad (14)$$

The optimization problem is challenging to be solved for several reasons: first, the dimension d of the input space to be found is not known *a priori*, but has to be determined. Second, given realistic signals, the number of features that can be extracted, and hence the size of the dictionary, can be quite large, leading to an optimization problem on a large dimensional space. To mitigate these difficulties, a greedy optimization strategy was adopted. The rationale is the following: we are interested in finding an input space of small dimension (to overcome the curse of dimensionality), and it is preferable that each input dimension is expressed as a sparse linear combination of the dictionary entries, to avoid overfitting problems. Henceforth, we start by defining an input space of dimension $d = 1$. For this, the weight matrix reduces to a vector. Assuming that only one dictionary entry can be used, an optimization is performed to choose the entry. Then, we look for a combination of two dictionary entries, and so on, till the score variation when adding an entry is less than a prescribed tolerance. When the first component of the input space x_1 is determined, we look for possible improvements by setting $d = 2$ and computing x_2 in the same way, when x_1 is the one found at the previous step of the algorithm. The greedy descent stops when the variation of the classification score is lower than an arbitrary tolerance. This double greedy strategy is defined in the pseudo-code Algorithm 2. The inner steps of the algorithm require the solution of a small size optimization problem, which is carried out by using a stochastic evolutionary strategy CMA-ES (presented in[32]).

Algorithm 2 Section Classification optimization: Sparse optimised classification.

1: F_s: dictionary matrix ▷ $F_s \in \mathbb{R}^{Ns \times Nb}$.
2: l: output vector ▷ Vector of size N_s.
3: $\mathbf{\Omega} = 0$ ▷ Initialize matrix of weights $\mathbf{\Omega} \in \mathbb{R}^{d \times Nb}$ with 0 values.
4: **for** $id = 1$ **to** d **do** ▷ Loop on the number of desired feature space dimension.
5: $V_{pos} = (1, 2, \ldots, N_b)$ ▷ Initialize the vector of the entries positions.
6: $N_{pos} = \#(V_{pos})$ ▷ Length of V_{pos}, number of available positions.
7: $\boldsymbol{\omega}_{id} = 0$ ▷ Vector of size N_b. Weights of the id^{th} dimension.
8: **for** $ic = 1$ **to** N_{comp} **do** ▷ Loop on the desired number of components to take into account for dimension id.
9: $p_{save}, \boldsymbol{\omega}_{save}$ ▷ Empty vectors. Store respectively best components position and best weights.
10: $\Omega_{save} = 0$ ▷ Empty matrix. Store best weights for all tested components. $\Omega_{save} \in \mathbb{R}^{ic \times Npos}$.
11: $s_{pos} = 0$ ▷ Vector with length of N_{pos}. Store computed cost.
12: **for** $ip = 1$ **to** N_{pos} **do** ▷ Loop on the number of available positions.
13: $\boldsymbol{\omega} = 0$ ▷ Initialize weight vector of size N_b.
14: $\boldsymbol{\omega}[p_{save}] = \boldsymbol{\omega}_{save}$ ▷ Initialize first components (if $ic > 1$).
15: $\boldsymbol{\omega}[V_{pos}[ip]] = 1$ ▷ Initialize the tested component.
16: $\mathbf{\Omega}[id,:] = \boldsymbol{\omega}$ ▷ Initialize the id^{th} dimension of the weights matrix.
17: **while** isConverged==False **do**

18: $M = F_s.\mathbf{\Omega}^T[:,: id]$ ▷ Classification input matrix $\boldsymbol{M} \in \mathbb{R}^{Ns \times id}$.
19: s_{Ns}=classification($\boldsymbol{M,l}$) ▷ Cost computation.
20: *isConverged* = checkConvergence ▷ Number of iterations, stagnation,...
21: $\omega[[p_{save}, V_{pos}[ip]]] = \omega_{new}$ ▷ CMA-ES. #(ω_{new}) = *ic*.
22: $\mathbf{\Omega}[id,:] = \omega$ ▷ Store weights.
23: $s_{pos}[ip]=s_{Ns}$ ▷ Store the computed cost.
24: $\Omega_{save}[:, ip] = \omega_{new}$
25: **end while**
26: **end for**
27: $p_{min} = argmin(s_{pos}[ip])$ ▷ Get the position of the best entry.
28: $p_{save} = (p_{save}, V_{pos}[p_{min}])$ ▷ Concatenate the position.
29: $\omega_{save} = \Omega_{save}[:, p_{min}]$ ▷ Get the best weights.
30: $V_{pos} = V_{pos} \backslash V_{pos}[p_{min}]$ ▷ Remove the position.
31: $N_{pos} = \#(V_{pos})$ ▷ (= N_{pos} − 1). Length of V_{pos}.
32: $\omega_{id}[p_{save}] = \omega_{save}$
33: **end for**
34: $\mathbf{\Omega}[id,:] = \omega_{id}$ ▷ Actualize the weights for the id^{th} dimension.
35: **end for**

The stopping criterion can be derived based on the analysis of the cost function. We propose to find the minimum variation which ensures that the classification does not change. It means that only the probabilities can differ between two consecutive cost computations without changing the predicted class. This corresponds to an increase of the margin between the classes. More details are given in Stop criterion based on the success rate variation (supplementary material).

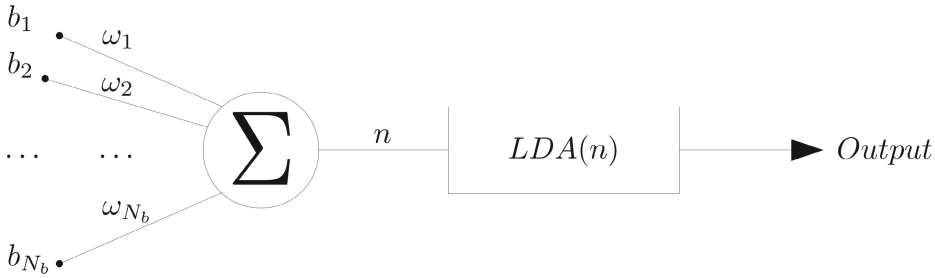

Figure 10. Optimised algorithm in one dimension interpreted as a neural network.

Remark: the presented algorithm can be interpreted as a simple perceptron[33] with one hidden layer as shown in Figure10 where all the weights are equal to zero except those selected by the algorithm. Instead of using usual activation function as sigmoid or Heaviside[34] we used the linear discriminant analysis (LDA) technique[35]. The analogy to the back propagation to compute the weights corresponds here to the CMA-ES algorithm. For a given set of weights, the obtained output is compared to the real solution through the cost function. Then a correction

is made on the weight until convergence. Figure11 shows the multidimensional case where the LDA classifier takes the different linear combinations computed for each dimension as input.

Cross-Validation

As inputs are computed to maximize the classification, a risk is to lose the generalization capacity of a good classifier. To prevent the overfitting and to increase the robustness of the strategy a random k-fold cross-validation was used. A stratification was applied on the data to ensure the conservation of the output repartition in each fold. The pseudo-code is described in Algorithm 3 and the corresponding Scikit-Learn method was used.

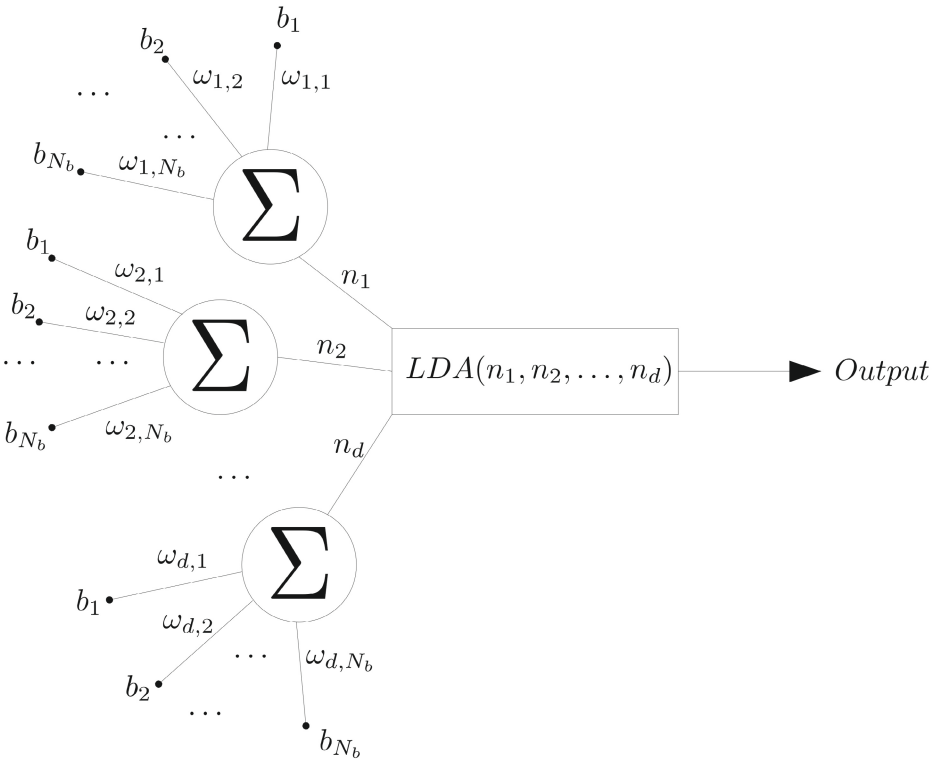

Figure 11. Optimised algorithm for d dimensions interpreted as a neural network.

Algorithm 3 Section Cross-Validation: Randomized K-fold cross-validation procedure.

1: *M*: input matrix
2: *l*: output vector
3: $N_{fold} = 2$ ▷ Number of folders for each K-Fold.
4: $N_{kfold} = 500$ ▷ Number of K-Fold.
5: $E = (1, 2, ..., N_s)$ ▷ Sample numbering.
6: $Cnt = 0$ ▷ Initialize counter vector of size N_s.

7: $P = 0$ ▷ Initialize matrix $\boldsymbol{P} \in \mathbb{R}^{Ns \times 2}$ with 0 values.
8: **for** $i \coloneqq 1$ **to** N_{kfold} **do**
9: $E' = getFolders(E, N_{fold}, l)$ ▷ Generate the N_{fold} folders with respect to the stratification.
10: **for** $j \coloneqq 1$ **to** N_{fold} **do**
11: $pos_{test} = E'[j]$ ▷ Testing folder (vector of indices).
12: $pos_{train} = E \setminus pos_{test}$ ▷ Complementary of pos_{test}.
13: $M_{train} = M[pos_{train},:]$ ▷ Extract train submatrice.
14: $l_{train} = l[pos_{train}]$ ▷ Extract train subvector.
15: $M_{test} = M[pos_{test},:]$ ▷ Extract test submatrice.
16: $l_{test} = l[pos_{test}]$ ▷ Extract test subvector.
17: clf = Train on (M_{train}, l_{train}) ▷ Train the classifier.
18: $proba$ = Test on (clf, M_{test}) ▷ Test the new data with the classifier.
19: $P[pos_{test},:] = P[pos_{test},:] + proba$ ▷ Add the new probabilities.
20: $Cnt[pos_{test}] = Cnt[pos_{test}] + 1$
21: **end for**
22: **end for**
23: **for** $i \coloneqq 1$ **to** N_s **do**
24: $P[i,:] = P[i,:]/Cnt[i]$ ▷ Compute averaged probability for the i^{th} sample.
25: **end for**

The repetition of the random K-fold strategy allows the convergence of the weights regardless of the training and test set generated. The higher the number of weights to determine, the higher should be the number of random K-fold.

Results

Two different studies were performed in the present work: classify compounds for their risk on TdP; classify compounds for their ion channel blocking properties. The results of these are presented hereafter.

In the first part of section "TdP classification", we describe the study results based on the conductance-block model (see Eq 7). Using this model, we classified the TdP risk of 86 known compounds based on simulated data using the compound's IC_{50} values for blocking sodium, potassium and calcium currents and the effective free therapeutic plasma concentration (EFTPC) values, reported by the literature.

In the second study (section "Channel classification") we classified compounds based on experimental data. The outcome consists in identifying which channel is affected (sodium, calcium or potassium) by a compound. These experiments were performed for 12 compounds using Pluricyte® Cardiomyocytes. Five of them were used for the training set and seven of

them for the validation. Because of the low sample size of data, a simulated database was generated to enrich the training set.

The stop criterion used for the following results is when the cost variation between the last two components is lower than 5%. The penalization parameter β described in Eq 13 was set to 0.1.

TdP classification

This section is dedicated to the torsadogenicity risk classification. Only simulated data are considered for this study. To predict the risk of TdP of a wide range of compounds, we simulated the application of 86 known compounds previously reported by[7].

Tests setup

The numerical choices leading to the results are summarised hereafter:

- The false positive part in the cost function (see Eq 11) was taken $\alpha = 2$, to minimise the false positive rate.

- Bidomain equation parameters are summarized in supplementary Table B.

- Drugs were modeled using Eq 7 presented in section "Drug modelling". The IC_{50} values for each compound are given in[13,36]. Concentrations chosen to simulate compounds are the effective free therapeutic plasma concentrations (EFTPC). These values are listed in supplementary Tables E and F. Eighteen drugs were modeled twice because of their different IC_{50} and EFTPC observed in the literature (see supplementary Tables E and F).

- The corresponding channels blocked in the ORd model are I_{Na} (g_{Na}), I_{Kr} (g_{Kr}) and calcium channels (I_{CaL}, I_{CaNa} and I_{CaK}) through the PCa variable as previously reported in[7].

- A 6-well MEA device (Multichannel Systems) with 9 electrodes per well (60-6wellMEA20030iR-Ti[37]) where the corresponding finite element mesh is presented in the left panel of Figure3. A cell heterogeneity field was applied on this finite element mesh following the strategy developed in section Heterogeneity.

- The sparse optimization was performed on a dataset of 1520 data points (76 first compounds, each compound simulated 20 times with different heterogeneities and sources). The FP traces corresponding to the last 10 compounds were also simulated 20 times with different heterogeneities and source, but used for the validation set. The same process was done for the calcium transient signals. The dictionary entries used for this classification problem are summarized in supplementary Table D.

Results of TdP classification

We start this section by commenting on the results of the classifier as function of the input space constructed by the greedy algorithm. In Figure12 the success rate of the classification for the validation set is plotted as function of the cost presented in section Classification optimization, Eq 11. The cost minimised by the proposed algorithm is a pertinent descriptor of the success rate of the classifier. The input space selected by progressively increasing the input space dimension as well as the components per dimension produces a high success rate. The input space corresponding to the case where the input is in $\mathbb{R}^2$ (with three dictionary components per direction) is shown in Figure12, from which we can appreciate that the separation between the classes is satisfactory.

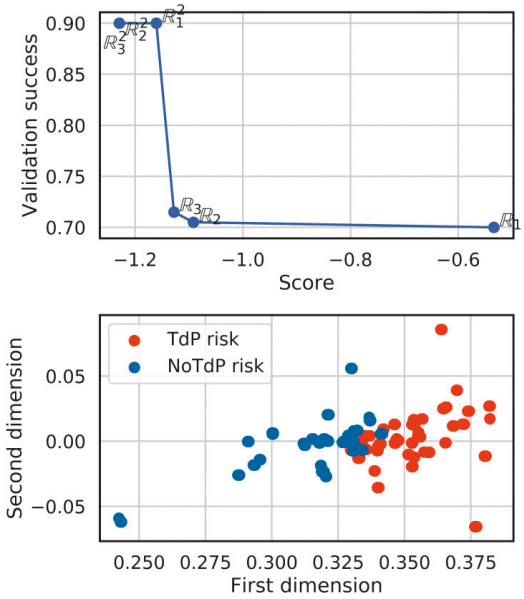

Figure 12. TdP risk classification through simulations of 86 compounds. *Top: Validation versus Cost curve depending on the number of components and the dimension. Bottom: Drug repartition in the input space after convergence of the algorithm.*

The results of the classification are detailed. In Figure13 the confusion matrices for the training set (left, in blue) and for the validation set (right, red) are shown. Globally, the results are similar for training and validation (no apparent overfitting phenomena were seen). The type II error (wrongly classifying a compound as non-torsadogenic) is well minimized thanks to the choice to penalize false positives ($\alpha = 2$ in the cost function, Eq 11). In the validation set, no compounds were wrongly classified as non-torsadogenic. Only the Propranolol was misclassified as torsadogenic (see supplementary Table E).

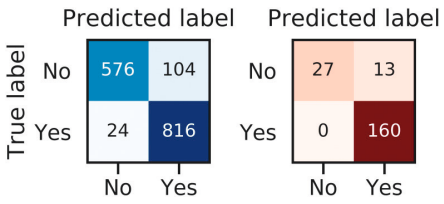

Figure 13. Confusion matrices obtained for TdP risk classification of 86 compounds after convergence of the algorithm. *Yes: TdP risk. No: No TdP risk. Left: Training set (sample size: 1520) using randomized K-fold cross-validation. Sensitivity = 0.98, Specificity = 0.85 and Accuracy = 0.92. Right: Validation set (sample size: 200). Sensitivity = 1, Specificity = 0.675 and Accuracy = 0.935.*

It is interesting to monitor the classification results at different stages of the algorithm. Confusion matrices obtained for test and validation sets show an improved TdP risk classification when we increase the number of components and dimensions. This improvement is particularly visible on the test set for the first components. The training on the first dimension is not sufficient to classify well the validation set. Meaning that other dictionary entries would have been selected by the algorithm (for the first dimension) if the validation set was in the training set. However, dictionary entries selected for the second dimension seem to be better to discriminate torsadogenic risk on the validation set.

Channel classification

This section is dedicated to the channel classification of 12 compounds based on *in vitro* data derived from MEA recordings of spontaneous beating hiPSC-CMs (Pluricyte® Cardiomyocytes) cultured on 96 well MEA plates (8 electrodes per well, Axion Biosystems), as described in section Cell culture. As we are limited by the experimental sample size (see compound list in supplementary Table 1), we enriched the experimental database with a simulated database (for which we know the classification output). For this study only FP traces were recorded and used for the training and classification, no calcium transient measurements were performed.

Tests setup

The numerical choices leading to the results are summarised hereafter:

- Bidomain equation parameters are summarized in supplementary Table C.

- Drugs were modeled using Eq 11 presented in section MEA computational model. The *in silico* database was generated blocking alternatively sodium (g_{Na}), potassium (g_{Kr}) or calcium (PCa) channels of the ORd model at a random percentage between 0% and 50%. Other channels are blocked between 0% to 5% to introduce some variability (e.g. blocking sodium at 35%, calcium at 2% and potassium at 3.5%). An example is shown in Figure14.

- The simulated sample size is 140 (computed from signals resulting from the simulation performed for different heterogeneity fields).

- A 96-well MEA device (Axion Bioystems) with 8 electrodes per well where the corresponding finite element mesh is presented in the right panel of Figure3. A cell heterogeneity field was applied on this finite element mesh following the strategy developed in section Heterogeneity.

The experimental data leading to the results are summarised hereafter:

- *In vitro* data used for this part are FP traces recorded from a hiPSC-CM monolayer (Pluricyte® Cardiomyocytes, Ncardia) plated on a 96 well MEA plate (8 electrodes per well) Axion Biosystems (Classic MEA 96 M768-KAP-96[38]).

- The 12 "CiPA" compounds listed in Table 1 were tested on Pluricyte® Cardiomyocytes and FP traces were recorded before and 30 minutes post compound addition. MEA results of 5 compounds were used for the training and MEA results of 7 "blind" compounds for the validation.

- Each compound was tested at 4 concentrations, 1 concentration per well and in 5 replicates (n = 5 per concentration).

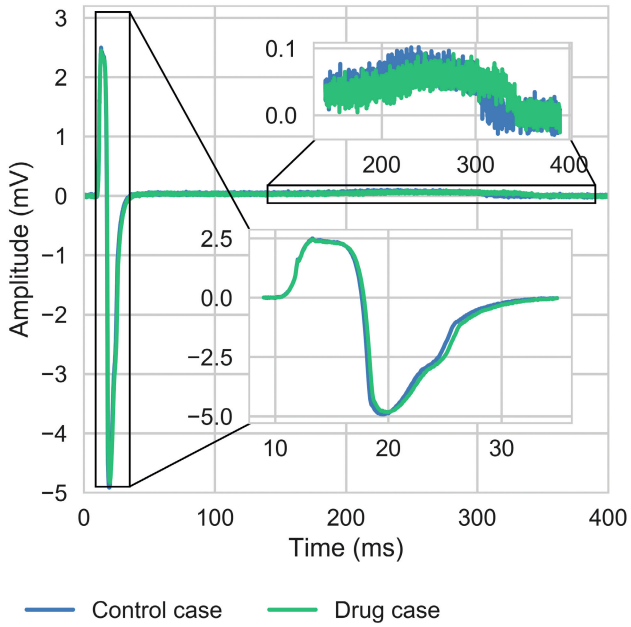

Figure 14. Section Channel classification: Simulated FP under control and compound conditions. *FP trace from one electrode, showing the effect of drug simulation blocking the sodium channel at 4%, calcium channels at 3.6% and potassium channel at 27.9%.*

The final experimental sample size was 75 for the training set and 85 for the validation set (some wells were removed from the analysis due to quiescence or noisy signal observations). The dictionary entry list is given in supplementary Table D. Using the conductance-block model described in Eq 7 we obtain the percentage of activity for each channel and concentration. This is shown in supplementary Table G. Two different kinds of classification problems have been studied: a binary classification (*i.e.* given a channel, is the molecule affecting its functioning), whose results are shown in section "Binary classification", and a ternary classification (*i.e.* is the molecule affecting potassium, calcium or sodium?), whose results are reported in section "Ternary classification". For the numerical experiments proposed, the success rate of the classifier for the training set was about 90%. In the following, we present in details the results on the *in vitro* data in the validation set.

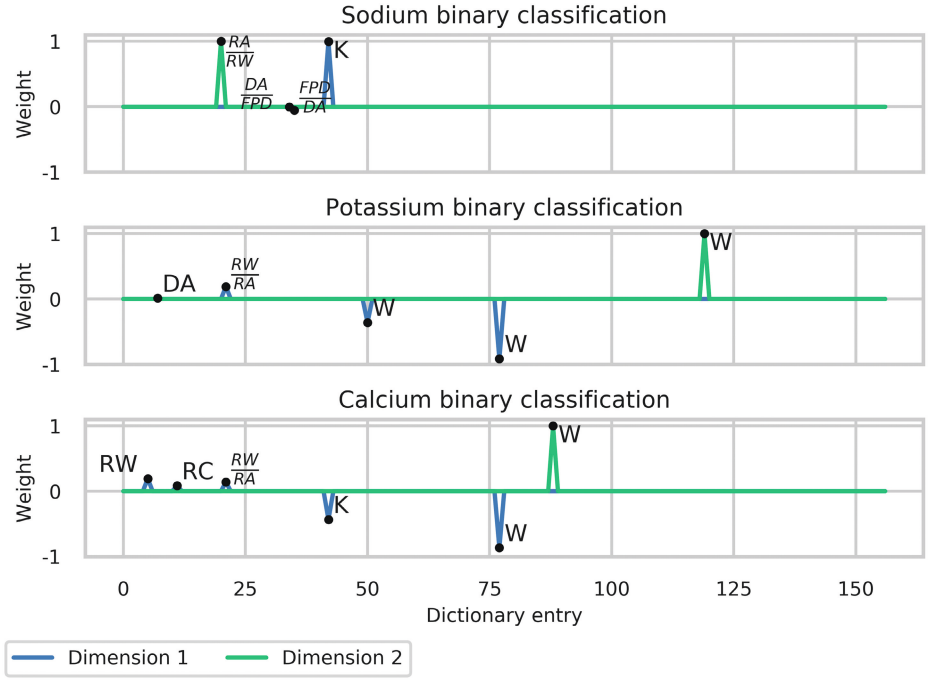

Figure 15. Weights obtained by the optimised classification algorithm.

Binary classification

We start this section by describing the outcome of the greedy algorithm selection. These are shown, for the three classification problems addressed, in Figure15, in which the weights of the dictionary entries are plotted. The selected entries are different (also in number) for the different classification problems. For instance, for the sodium binary classification, we obtained 3 components for the dimension 1 whereas for the same dimension, we obtained 4 components for the potassium case and 5 for the calcium case. In all the cases, the linear combinations retained are sparse.

The classification results are reported hereafter. First, an aggregated result is presented (considering all the different concentrations, providing an overall label). Then, in the last part of this section, the results at different concentrations are described.

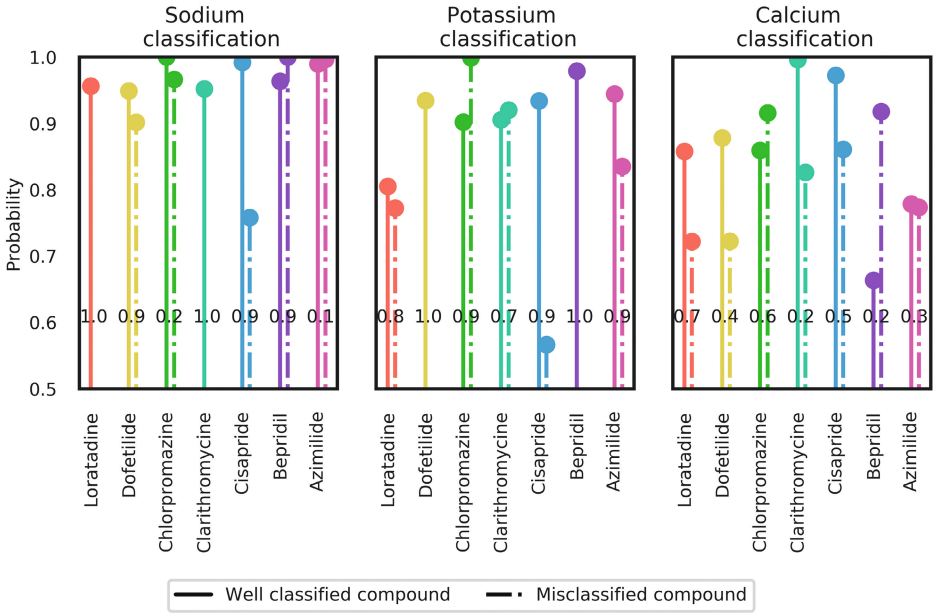

Figure 16. Experimental data classification in binary case. *Plain (resp. dotted) lines correspond to the average confidence of the LDA classifier for well classified (resp. misclassified) compound (well classification is according to Table 1). The black values on the lines correspond to the proportion of well classified observations for each compound.*

Binary classification: Aggregated result

Figure16 shows classification results for the seven compounds that were included in the validation set. The value shown for each compound corresponds to the success rate of classifying the compound correctly as a blocker or non-blocker for either the sodium, potassium or calcium channel according to their label (see Table 1).

The results for the 7 molecules in the validation set are commented:

1. Loratadine: *potassium and calcium channel blocker* (Table 1)

For the sodium channel block classification, Loratadine is always well classified (as a non-sodium channel blocker) with high confidence (averaged probability returned by the classifier is close to one, see Figure16). For potassium blockade, Loratadine is well classified in 80% of the cases. Moreover, when Loratadine is well classified, the classifier is more confident (> 0.8) than when it is misclassified (< 0.8).

2. Dofetilide: *potassium channel blocker* (Table 1)

The classifier always returns Dofetilide as a potassium channel blocker with a high probability. Dofetilide is also classified as a sodium blocker, but only for 10% of the cases and with a lower probability than when it is not classified as a sodium blocker. For the calcium channel block classification, Dofetilide is considered as a non-calcium channel blocker for 40% of the cases but with a higher probability than when it is considered as a calcium channel blocker.

3. Chlorpromazine: *potassium, calcium and sodium channel blocker* (Table 1)

Chlorpromazine is well classified for the potassium and calcium channel classifications (i.e. it is considered as a potassium channel blocker and calcium channel blocker). The success rates for Chlorpromazine are similar to those obtained with Loratadine. An explanation might be the fact that they approximately have the same factor between the hERG and Cav1.2 IC_{50} values. In addition, Chlorpromazine is classified as a sodium channel blocker in only 20% of all cases, but with a probability of 100%.

4. Clarithromycine: *potassium channel blocker* (Table 1)

Clarithromycine is well considered as a non-sodium channel blocker with a high confidence and for all tested samples. In 70% of the cases Clarithromycine is well classified as a potassium channel blocker with around 90% of confidence. However, Clarithromycine is also labeled as a calcium blocker for 80% of the samples and with more than 80% of confidence. Important to note here is that, although Clarithromycine is labeled as a non-calcium channel blocker for only 20% of the samples, the confidence for this well classification is close to 100%.

5. Cisapride: *potassium channel blocker* (Table 1)

If we compare classification results obtained for Chlorpromazine and Cisapride, the potassium channel binary classification success rate is the same. However, the classifier is more confident when Cisapride is well classified. Moreover, for the calcium channel classification, Chlorpromazine is classified as a calcium channel blocker in 60% of the cases whereas Cisapride is classified as non-calcium channel blocker in 50% of the cases with a higher confidence than when Cisapride is misclassified as calcium channel blocker. Moreover, in 90% of the samples tested, Cisapride is being classified as a non-sodium channel blocker with a confidence close to 100%. These results are in good agreement with the high potency of Cisapride to block the hERG channel, and the multi-channel block ability (hERG, Nav1.5 and Cav1.2) for Chlorpromazine.

6. Bepridil: *potassium, calcium and sodium channel blocker* (Table 1)

Sodium and potassium channel blockade classification for Bepridil is well captured by the classifier (with high proportion and high confidence). Calcium channel blockade is not seen by the classifier for Bepridil. A potential explanation could be that if calcium and potassium

channels are blocked simultaneously, Bepridil does not show a specific pattern of a calcium channel blocker, but essentially potassium and sodium channel patterns are detected as shown in Figure 17 (e.g FPD prolongation due to potassium channel block and DA decrease due to sodium channel block).

7. Azimilide: *potassium, sodium and calcium channel blocker* (Table 1)

Azimilide is well classified as a potassium channel blocker with a high confidence and for 90% of the sample. The sodium channel blockade by Azimilide is clearly not seen by the classifier as 90% of the sample is labeled as non-sodium channel blockade with a confidence close to 100%. The calcium channel blockade classification is also less clear as only 70% of the samples are labeled as non-calcium channel blockade with almost 80% of confidence. This could be related to the potency of Azimilide to block the inward sodium currents and L-type calcium channels is lower than for blocking the hERG channel[52]. Besides, the highest concentration tested was lower than the IC_{50} values for blocking sodium and calcium channels (Table 1). A dictionary entry chosen by the algorithm for potassium and calcium blockade classification is the ratio *RW/RA* (see Figure 15). As shown in[53], hERG channel block can induce a T-wave flattening in the ECG. This phenomenon is also observed in the FP repolarization of Pluricyte® Cardiomyocytes for 0.1 *μM* of Bepridil (see Figure 17) and could be an explanation of the *RW/RA* selection by the algorithm.

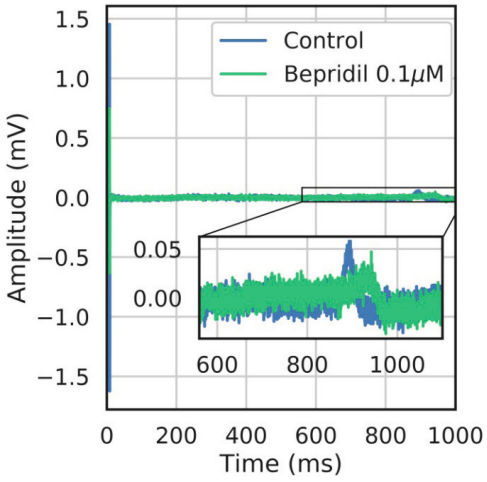

Figure 17. Example of experimental data with Bepridil, showing an increase in FPD and a decrease in DA of Pluricyte® Cardiomyocytes.

For most of the cases, drugs are well classified with a high confidence. However, this is not always the case. For instance, Dofetilide has been perfectly classified as a potassium channel blocker with a high confidence (around 90%), but Dofetilide has also been misclassified as a calcium channel blocker with a high confidence (around 70%).

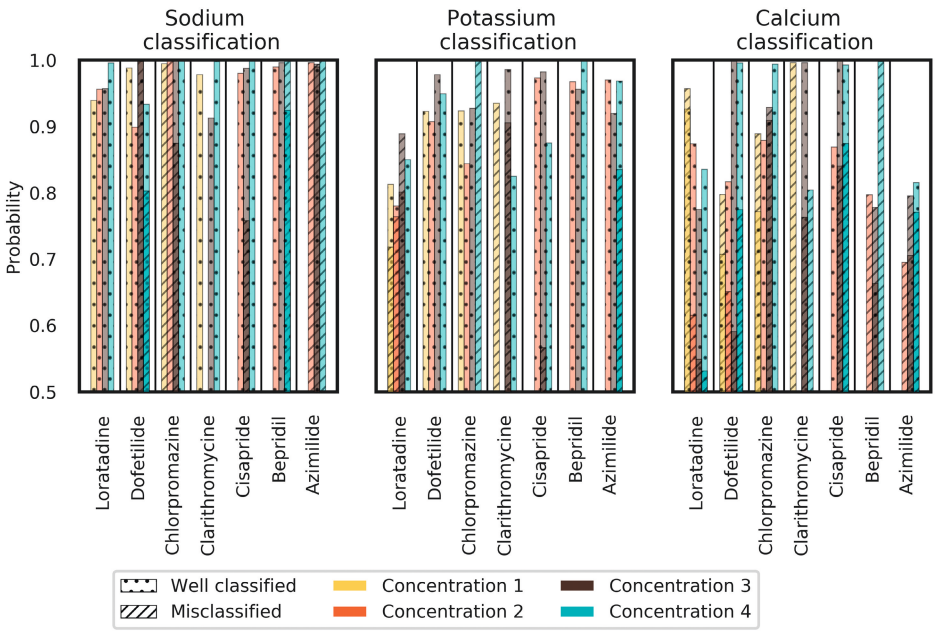

Figure 18. Experimental data classification in binary case for each concentration. *Some concentrations were not used due to the quiescence or noisy signal observation. For each concentration, the LDA classifier returns the average probability for well classified (dotted bars) and misclassified (hatched bars) compounds.*

5

Binary classification: Study for each concentration

Details for ion channel block classification of each concentration of each compound are given in Figure18. This figure shows how each compound was classified at each concentration. The interest is to study the evolution of the classification with respect to increasing concentrations. As done in the previous section, we present the results for each of the 7 molecules in the validation set.

1. Loratadine: *potassium and calcium channel blocker* (Table 1)

We know from Figure16 that Loratadine is always classified as a non-sodium channel blocker. From Figure18 we can conclude that the confidence of Loratadine being a non-sodium channel blocker increases with higher concentrations. In addition, Loratadine has also been classified as a potassium channel blocker in 80% of the cases (see Figure16). Figure18 shows that the classification is the best at the highest concentration (no misclassification), which can be explained by the relatively low test concentrations compared to the IC_{50} values (Table 1). Moreover, for the first two concentrations in the potassium channel classification, the confidence is higher when Loratadine is well classified than when Loratadine is misclassified. A bad mark is the increase of the misclassified confidence for the first three concentrations. However, for the highest concentration tested, none of the samples were misclassified.

Concerning the classification for the calcium channel, the success rate of Loratadine to be classified as a calcium channel blocker was 70% (Figure16); and based on Figure18 we can conclude that the misclassified confidence decreases strongly when the concentration increases. This is in line with the differences seen in IC_{50} values between hERG, Cav1.2 and Nav1.5 (Table 1).

2. Dofetilide: *potassium channel blocker* (Table 1)

Dofetilide was wrongly labeled as a calcium channel blocker in 60% of the cases (see Figure16). However, the well-classified confidence increases strongly with the concentration (see Figure18), which means that the confidence of Dofetilide being a calcium channel blocker decreases when the concentration increases. The well-classified probability for the sodium channel (Dofetilide being a non-sodium channel blocker) and potassium channel (Dofetilide being a potassium channel blocker) is around 90% or even higher for all concentrations tested.

3. Chlorpromazine: *potassium, calcium and sodium channel blocker* (Table 1)

Chlorpromazine is known to block sodium, potassium and calcium channels (see Table 1). Only for the first three concentrations, Chlorpromazine is clearly seen as a potassium channel blocker (Figure18). The fourth and highest concentration show that sodium and calcium channels are affected instead of potassium. This is in line with the different potencies of Chlorpromazine for the different ion channels: Chlorpromazine blocks hERG more potently than sodium or calcium (see Table 1). The calcium channel blockade is confirmed by the fact that well-classified confidence for calcium channel block increases with concentration, in addition to being well classified in 60% of all cases.

4. Clarithromycine: *potassium channel blocker* (Table 1)

Clarithromycine is better classified as a potassium channel blocker at higher concentrations (higher confidence for the third concentration and no misclassification for the fourth concentration). Also the sodium classifier shows us that for all test concentrations, Clarithromycine is well classified as a non-sodium channel blocker. However, for any concentration, the calcium classifier does not give us satisfactory results, which means that Clarithromycine is wrongly classified as a calcium channel blocker.

5. Cisapride: *potassium channel blocker* (Table 1)

Well-classified confidence for Cisapride is always higher than misclassified confidence regardless of the concentration and, particularly for the sodium and potassium channel classifiers. This is in line with Cisapride being a very potent potassium blocker (see Table 1).

6. Bepridil: *potassium, calcium and sodium channel blocker* (Table 1)

Bepridil is well classified as a sodium and potassium channel blocker with a high confidence. This is not the case for the calcium classification. An explanation could be that the potassium channel blockade hides the effect of the calcium channel blockade as above mentioned.

7. Azimilide: *potassium, sodium and calcium channel blocker* (Table 1)

Azimilide is classified as a potassium channel blocker with a probability higher than 90% for all concentrations tested. However Azimilide is misclassified for sodium and calcium channel blockade. As abovementioned, this could be related to the fact that Azimilide blocks the inward sodium currents and L-type calcium channels at concentrations 5-10 times higher than required for blocking the hERG channel[52].

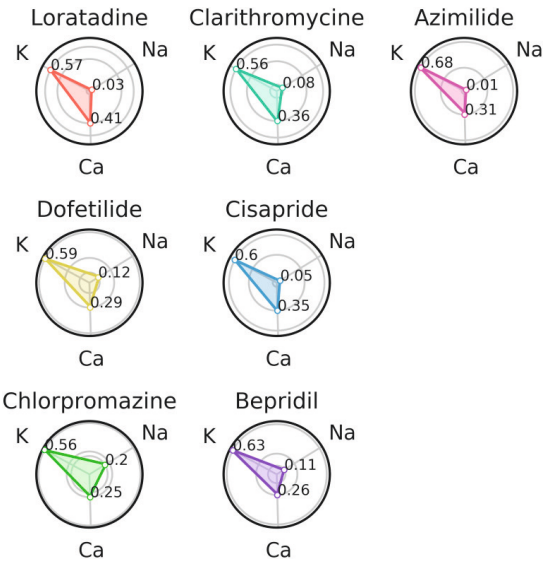

Figure 19. Experimental data classification in ternary case.

Ternary classification

For the ternary classification we only considered one classifier but with three outputs: sodium, potassium and calcium channel blockers. Aggregated results for the ternary classification are presented in Figure19. The ternary classifier classified all seven compounds from the validation set as potassium channel blockers. As expected, the probability returned by the classifier decreases when the IC_{50} value increases (for example the probability for Loratadine to be a calcium channel blocker is 0.41 with IC_{50} = 11.4 μM (see Table 1) and the probability for Dofetilide to be a calcium channel blocker is 0.29 with IC_{50} = 26.7 μM (see Table 1)). These results do not take into account the different concentrations tested. The probabilities given for each concentration are given in Figure20.

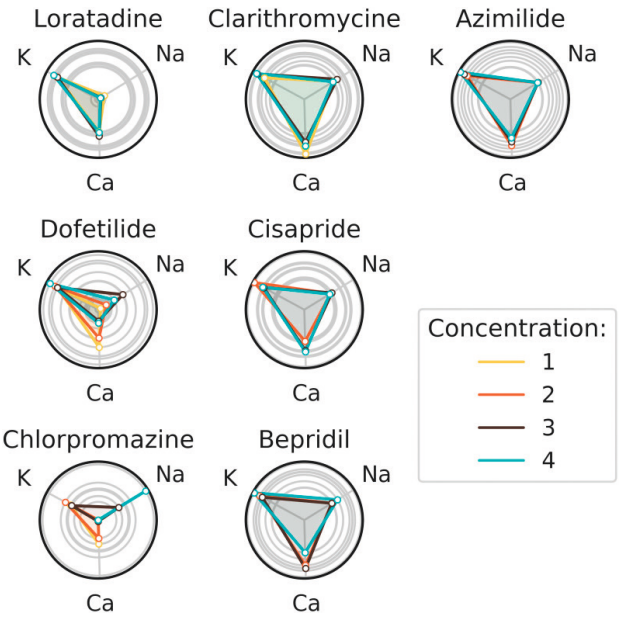

Figure 20. Experimental data classification in ternary case for each concentration.

The results for each of the 7 molecules are detailed hereafter. For sake of brevity, both aggregated and by-concentration results are commented.

1. Loratadine: *potassium and calcium channel blocker* (Table 1)

Loratadine is well classified as a potassium channel blocker with a probability equals to 0.57 (Figure19). The second highest probabilty concerns the calcium channel blocker, which was expected as Loratadine is more potent to block hERG (6.1 *μM*, see Table 1) than to block the L-type calcium channel (11.4 *μM*, see Table 1). Figure20 shows us that the confidence of the classifier is almost the same regardless to the concentration.

2. Dofetilide: *potassium channel blocker* (Table 1)

From Figure19, we can see that Dofetilide is well classified as a potassium channel blocker with a probability equals to 0.59. If we now look at the classification results of Dofetilide in Figure20, a high concentration gives a higher probability of being a potassium channel blocker and a lower probability to be a calcium channel blocker (which is in line with the binary classification method presented in Figure17). This can be explained by the fact that for the three lower concentrations, the potassium activity is always higher than 90%(see supplementary Table G) whereas the highest concentration corresponds to a 75% activity (see supplementary Table G).

3. Chlorpromazine: *potassium, calcium and sodium channel blocker* (Table 1)

Chlorpromazine is well classified as a potassium channel blocker with a probability equals to 0.56 (Figure19). The probabilities for Chlorpromazine of being a calcium or sodium channel blocker are close to each other (Figure19), which was expected as the IC_{50} values for calcium and sodium channel blockade are close to each other as well (Table 1). The confidence to classify Chlorpromazine as a sodium channel blocker is the highest for the highest concentration tested (3 *μM*, see Table 1) (Figure20). An explanation of this result could be that some compensation effects would appear on the repolarization due to the simultaneous block of potassium as well as calcium. 3*μM* of Chlorpromazine corresponds at a 50% activity of the sodium channel (see conductance-block model in section Drug modeling), which is clearly visible on the depolarization amplitude (see Figure21).

4. Clarithromycine: *potassium channel blocker* (Table 1)

Clarithromycine is well classified as a potassium channel blocker with a probability equals to 0.56. It is interesting to see that the confidence of being a calcium channel blocker is lower for Clarithromycine than for Loratadine (see Figure19). This point is expected because Loratadine is known to block calcium channels with an IC_{50} of 11.4 *μM* (see Table 1), which is not the case for Clarithromycine (IC_{50} > 30 *μM*). Another good point is that the confidence of being a potassium channel blocker for Clarithromycine slightly increases with higher concentrations (Figure20).

5. Cisapride: *potassium channel blocker* (Table 1)

Cisapride is well classified as a potassium channel blocker with a probability equals to 0.6 (see Figure19). The second highest confidence is for the calcium channel blocker. These channel blockade probabilities are in good agreement with the IC_{50} values of Cisapride for potassium channel blockade (0.02 *μM*) and calcium channel blockade (11.8 *μM*) (Table 1). The difference in these values might also explain the observation that the confidence of being a potassium channel blocker decreases when the concentration increases, following by a higher confidence of Cisapride being a calcium channel blocker (Figure20).

6. Bepridil: *potassium, calcium and sodium channel blocker* (Table 1)

Bepridil is well classified as a potassium channel blocker with a probability equals to 0.63 (see Figure19). The order of the different ion channel blockade probabilities is in good agreement with the IC_{50} values order (Table 1). The sodium channel blockade probability is 0.11. This probability is coherent in the sense that Bepidril is known to block the sodium channel; other compounds which are not known as sodium channel blockers have a lower probability (0.01-0.08) of being a sodium channel blocker (except for Dofetilide at low concentrations).

Unexpectedly, Figure19 shows that the probability to be a calcium channel blocker is similar between Bepridil and Dofetilide (not a calcium channel blocker). Even for the last concentration of Bepridil, there is a decreasing confidence of being a calcium channel blocker in favor of being a potassium and sodium channel blocker (Figure20). This could be explained by the fact that Bepridil has a higher potency for blocking hERG compared to blocking calcium channels and that the effects of hERG channel blockade masked the effects of blocking calcium channels.

7. Azimilide: *potassium, sodium and calcium channel blocker* (Table 1)

Azimilide is well classified as a potassium blocker with a probability of 0.68 (see Figure19). Although it is known that the potency of Azimilide to block the inward sodium currents and L-type calcium channels is lower than blocking the hERG channel, the probability of being a sodium channel blocker was still lower than expected and did not change with higher concentrations.

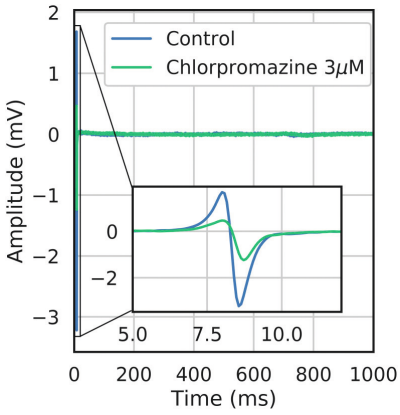

Figure 21. Example of experimental FP trace with Chlorpromazine.

Discussion

Human iPSC-CMs are being increasingly adapted as a novel *in vitro* model to better recapitulate human heart function and to complement or replace existing *in vitro* assays for improved cardiac safety assessment. Of the many studies that have now investigated the impact of drugs on the electrophysiology of hiPSC-CMs, the most well-known is the multisite CiPA initiative. Data presented in[6] describe the utility of hiPSC-CMs in combination with MEA and voltage-sensing optical methods in evaluating the electrophysiological responses to 28 drugs linked to low, intermediate, and high TdP risk categories. Studies like the CiPA multisite study show promising results. However, predicting TdP risk at a reasonable level of accuracy remains a challenge. Besides, many screening platforms, like various MEA and calcium-flux devices, are becoming increasingly sophisticated and generate large multidimensional datasets. Improved

automated analysis methods, including classification methods to accurately predict the risk for ion-channel block and TdP, are needed.

In the present work, a preliminary step towards the setup of high-throughput screening procedures was attempted. In particular, a method was proposed to systematically deal with classification problems involving "CiPA" compounds for their risk to induce TdP as well as for their ion channel blocking properties.

Algorithm

The algorithm developed in this study selects and combines pertinent features extracted from the signals in order to maximize the classification score (both in terms of the success rate and the confidence of the classifier) by means of a double greedy optimization. The algorithm promotes sparsity (hence mitigating the overfitting risk) and it is fully scalable in terms of parallelism (remark that the number of cores can potentially equal the dictionary entry size). In this paper, the input space computed by the algorithm maximize a score by linearly separating the classes samples, using the classical LDA method. It would be interesting to test the algorithm with other classifiers such as support vector machine (SVM) with different kernels or k nearest neighbor (KNN) and against classification with PCA.

We applied the algorithm on simulated FP and calcium transient data for TdP risk classification as well as on *in vitro* data coming from FP signals recorded from hiPSC-CMs (Pluricyte® Cardiomyocytes) that were cultured on 96 well MEA plates and subjected to 12 CiPA reference compounds (5 compounds were used as a training set and 7 were used to validate the algorithm).

TdP risk assessment

The classifiers obtained have given encouraging results for a drug safety profile of the compounds. Compounds known to have a high TdP risk were 100% well classified according to the arrhythmogenicity risk classification and a compound known to have a low TdP risk was well classified in 67% of the cases. This is conforming to the fact that we decided to put a strong weight on the type II error (wrongly classify a compound as non-torsadogenic). Concerning the torsadogenicity classification, more tests have to be done with higher concentrations (10xEFTPC, 50xEFTPC, etc). Thus, the compound impact on physiological traces (FP and intracellular calcium transient) would be more important, which would improve the classification (bigger margin between the data points and the separation plan). However, even at EFTPC, the TdP risk classification results are encouraging as only Propranolol was misclassified as torsadogenic. Particularly, the algorithm allows us to weight the type II error. To improve the arrhythmogenicity assessment, a ternary classifier could be established to distinguish low, moderate or high TdP risk.

Ion-channel blockade

Concerning ion-channel blockade classification of compounds, potassium was always well classified with a high confidence. Moreover, for the ternary classification study, for most of the tested compounds, the lower the IC_{50} for a channel, the higher the confidence of the classifier to block this channel. The binary sodium channel blockade classification is good for all the compounds except for Chlorpromazine (at low concentration). The ternary classification study shows similar probabilities of Chlorpromazine for blocking the sodium channel as for blocking the calcium channel, which is in agreement with the similar IC_{50} values of Chlorpromazine for these channels. However, the binary classification is less good for the calcium channel blockade classification. This could also be related to the fact that all CiPA compounds from the validation set block the hERG channel and with higher potencies compared to blocking the calcium channel. The effect of blocking hERG could mask the effect of blocking calcium, making calcium channel blockade more difficult to classify. In general, the binary and ternary classification strategies are in a good agreement (e.g potassium channel blockade is always well classified).

Nevertheless, more tests have to be done on the algorithm in order to validate and/or improve the classifiers. For the channel block classification, simulations have been done only on highly pure channel block properties (no multi-channel blockade), simplified to only three types of channels: potassium, calcium or sodium, which is often not representative of the total ion channel blocking effects a compound could have. Training based on *in silico* multi-channel blockade would be more realistic and would most likely increase the robustness of the classification. Moreover, the present experimental protocol was performed at different concentrations for each compound. The dictionary entry could take this information into account.

Each application presented in this paper was based on one specific model of MEA device. It would also be interesting to know whether the MEA device might have an impact on the analysis of the drug effect, *i.e.* to study the case where we learn with one MEA device and we validate with data coming from another MEA device.

The addition of intracellular calcium transient data would increase the classification in order to identify not only effects on ion-channels but also to detect negative and positive inotropic effects thereby having the capability to classify other classes of compounds, such as calcium-sensitizers or adrenergic receptor agonists.

The time compound dynamic was not studied in this paper. The dictionary could be extended with new biomarkers as beat rate or depolarization standard deviation. These new entries could provide information on the impact of the compound on the monolayer stability. In order to represent this behavior in the *in silico* dataset, a pacemaker action potential model showing experimental beat rate behavior (Paci *et al*[54]) could be introduced.

In summary, the algorithm that we developed proved to be a promising tool to classify compounds for their risk to induce TdP as well as for their ion-channel blocking properties based on *in vitro* and in silico data derived from hiPSC-CMs. Therefore, this method can be implemented in *in vitro* MEA and/or calcium-flux studies using hiPSC-CMs where it may serve as a tool to improve machine learning approaches and to deliver fast and reliable prediction of drug-induced ion channel blockade and proarrhythmic behavior to advance cardiac safety assessment.

Funding Statement

T.K: FDA Broad Agency Announcement (BAA) contract (FDABAA-15-00121) to the Health and Environmental Sciences Institute (HESI) and partly through federal funds from the National Center Institute (number HHSN261200800001E) and European Union's Horizon 2020 (number 726513). https://www.fda.gov/https://hesiglobal.org/https://ec.europa.eu/programmes/horizon2020/en The funders had no role in study design, data collection and analysis, decision to publish, or preparation of the manuscript.

Data Availability

Data/Code are available on the following github repository: fraphel/fp_gen (field potential simulations) and fraphel/TdP_Channel_Classification (Classification).

Acknowledgements

We would like to thank NOTOCORD/Instem for their help to establish relationship and colaborations between Ncardia and Inria.

References

1. Crumb WJ, Vicente J, Johannesen L, Strauss DG. An evaluation of 30 clinical drugs against the comprehensive *in vitro* proarrhythmia assay (CiPA) proposed ion channel panel. Journal of pharmacological and toxicological methods. 2016;81:251–262. 10.1016/j.vascn.2016.03.009
2. Millard D, Dang Q, Shi H, Zhang X, Strock C, Kraushaar U, et al. Cross-site reliability of human induced pluripotent stem-cell derived cardiomyocyte based safety assays using microelectrode arrays: Results from a blinded CiPA pilot study. Toxicological Sciences. 2018; p. kfy110. 10.1093/toxsci/kfy110
3. Yamazaki D, Kitaguchi T, Ishimura M, Taniguchi T, Yamanishi A, Saji D, et al. Proarrhythmia risk prediction using human induced pluripotent stem cell-derived cardiomyocytes. Journal of pharmacological sciences. 2018;136(4):249–256. 10.1016/j.jphs.2018.02.005
4. Dutta S, Chang KC, Beattie KA, Sheng J, Tran PN, Wu WW, et al. Optimization of an *in silico* cardiac cell model for proarrhythmia risk assessment. Frontiers in Physiology. 2017;8:616 10.3389/fphys.2017.00616
5. Pugsley MK, Harter ML, de Korte T, Connaughton C, Authier S, Curtis MJ. Safety pharmacology methods and regulatory considerations evolve together; 2018.
6. Blinova, Ksenia and Dang, Qianyu and Millard, Daniel and Smith, Godfrey and Pierson, Jennifer and Guo, Liang and Brock, Mathew and Lu, Hua Rong and Kraushaar, Udo and Zeng, Haoyu and others International multisite study of human-induced pluripotent stem cell-derived cardiomyocytes for drug proarrhythmic potential assessment. In: Cell reports 3582–3592.
7. Cummins Lancaster M, Sobie E. Improved Prediction of Drug-Induced Torsades de Pointes Through Simulations of Dynamics and Machine Learning Algorithms. Clinical Pharmacology & Therapeutics. 2016;100(4):371–379. 10.1002/cpt.367
8. Passini E, Britton OJ, Lu HR, Rohrbacher J, Hermans AN, Gallacher DJ, et al. Human *in silico* drug trials demonstrate higher accuracy than animal models in predicting clinical pro-arrhythmic cardiotoxicity. Frontiers in physiology. 2017;8:668 10.3389/fphys.2017.00668
9. Bortolan G, Willems J. Diagnostic ECG classification based on neural networks. Journal of Electrocardiology. 1993;26:75–79.
10. Asl BM, Setarehdan SK, Mohebbi M. Support vector machine-based arrhythmia classification using reduced features of heart rate variability signal. Artificial intelligence in medicine. 2008;44(1):51–64. 10.1016/j.artmed.2008.04.007
11. Tung L. A bi-domain model for describing ischemic myocardial D–C potentials. MIT; 1978.
12. O'Hara T, Virág L, Varró A, Rudy Y. Simulation of the undiseased human cardiac ventricular action potential: model formulation and experimental validation. PLoS computational biology. 2011;7(5):e1002061 10.1371/journal.pcbi.1002061
13. Mirams G, Cui Y, Sher A, Fink M, Cooper J, Heath B, et al. Simulation of multiple ion channel block provides improved early prediction of compounds clinical torsadogenic risk. Cardiovascular research. 2011;91(1):53–61. 10.1093/cvr/cvr044
14. Zemzemi N, Bernabeu M, Saiz J, Cooper J, Pathmanathan P, Mirams G, et al. Computational assessment of drug-induced effects on the electrocardiogram: from ion channel to body surface potentials. British journal of pharmacology. 2013;168(3):718–733. 10.1111/j.1476-5381.2012.02200.x
15. Bottino D, Penland RC, Stamps A, Traebert M, Dumotier B, Georgieva A, et al. Preclinical cardiac safety assessment of pharmaceutical compounds using an integrated systems-based computer model of the heart. Progress in biophysics and molecular biology. 2006;90(1):414–443. 10.1016/j.pbiomolbio.2005.06.006
16. Zwartsen, Anne and de Korte, Tessa and Nacken, Peter and de Lange, Dylan W and Westerink, Remco HS and Hondebrink, Laura Cardiotoxicity screening of illicit drugs and new psychoactive substances (NPS) in human iPSC-derived cardiomyocytes using microelectrode array (MEA) recordings. Journal of molecular and cellular cardiology 136. 102–112. 2019 Elsevier

17. Colatsky T, Fermini B, Gintant G, Pierson JB, Sager P, Sekino Y, et al. The comprehensive *in vitro* proarrhythmia assay (CiPA) initiative-Update on progress. Journal of pharmacological and toxicological methods. 2016;81:15–20. 10.1016/j.vascn.2016.06.002
18. Raphel F, Boulakia M, Zemzemi N, Coudière Y, Guillon JM, Zitoun P, et al. Identification of ion currents components generating field potential recorded in MEA from hiPSC-CM. IEEE Transactions on Biomedical Engineering. 2017.
19. Hindmarsh AC, Brown PN, Grant KE, Lee SL, Serban R, Shumaker DE, et al. SUNDIALS: Suite of nonlinear and differential/algebraic equation solvers. ACM Transactions on Mathematical Software (TOMS). 2005;31(3):363–396. 10.1145/1089014.1089020
20. Abbate E, Boulakia M, Coudière Y, Gerbeau JF, Zitoun P, Zemzemi N. *In silico* assessment of the effects of various compounds in MEA/hiPSC-CM assays: Modelling and numerical simulations. Inria, https://hal.inria.fr/hal-01562673; 2017. Available from: https://hal.inria.fr/hal-01562673.
21. Chapelle, Dominique and Collin, Annabelle and Gerbeau, Jean-Frederic A surface-based electrophysiology model relying on asymptotic analysis and motivated by cardiac atria modeling. Mathematical Models and Methods in Applied Sciences 2749–2776.
22. Schenone Elisa and Collin Annabelle and Gerbeau Jean-Frederic Numerical simulation of electrocardiograms for full cardiac cycles in healthy and pathological conditions. International journal for numerical methods in biomedical engineering
23. Tarabelloni Nicholas and Schenone Elisa and Collin Annabelle and Ieva Francesca and Paganoni Anna Maria and Gerbeau Jean-Frederic Statistical Assessment and Calibration of Numerical ECG Models. JP Journal of Biostatistics 151–173.
24. Tixier E, Raphel F, Lombardi D, Gerbeau JF. Composite biomarkers derived from Micro-Electrode Array measurements and computer simulations improve the classification of drug-induced channel block; 2017. https://hal.archives-ouvertes.fr/hal-01570819.
25. Bowler Louise A and Gavaghan David J and Mirams Gary R and Whiteley Jonathan P. Representation of multiple cellular phenotypes within tissue-level simulations of cardiac electrophysiology. Bulletin of mathematical biology. 2019, vol. 81, no 1, p. 7–38. 10.1007/s11538-018-0516-1
26. Chang Kelly C and Dutta Sara and Mirams Gary R and Beattie Kylie A and Sheng Jiansong and Tran Phu N and Wu Min and Wu Wendy W and Colatsky Thomas and Strauss David G and others Uncertainty quantification reveals the importance of data variability and experimental design considerations for in silico proarrhythmia risk assessment. Frontiers in physiology, 2017, vol. 8, p. 917 10.3389/fphys.2017.00917
27. Nakamura Y, Matsuo J, Miyamoto N, Ojima A, Ando K, Kanda Y, et al. Assessment of testing methods for drug-induced repolarization delay and arrhythmias in an iPS cell–derived cardiomyocyte sheet: Multi-site validation study. Journal of pharmacological sciences. 2014;124(4):494–501. 10.1254/jphs.13248FP
28. Chang PC, Wo HT, Lee HL, Lin SF, Wen MS, Chu Y, et al. Role of sarcoplasmic reticulum calcium in development of secondary calcium rise and early afterdepolarizations in long QT syndrome rabbit model. PloS one. 2015;10(4):e0123868 10.1371/journal.pone.0123868
29. Tertoolen L, Braam S, van Meer B, Passier R, Mummery C. Interpretation of field potentials measured on a multi electrode array in pharmacological toxicity screening on primary and human pluripotent stem cell-derived cardiomyocytes. Biochemical and biophysical research communications. 2018;497(4):1135–1141. 10.1016/j.bbrc.2017.01.151
30. Bellman RE. Adaptive control processes: a guided tour. vol. 2045 Princeton university press; 2015.
31. Saeys Y, Inza I, Larrañaga P. A review of feature selection techniques in bioinformatics. bioinformatics. 2007;23(19):2507–2517. 10.1093/bioinformatics/btm344
32. Hansen N. The CMA evolution strategy: a comparing review In: Towards a new evolutionary computation. Springer; 2006. p. 75–102.
33. Blue LM, Bauer KW Jr. Determining input features for multilayer perceptrons. Neurocomputing. 1995;7(2):111–121. 10.1016/0925-2312(94)E0053-T

34. Widrow B, Lehr MA. 30 years of adaptive neural networks: perceptron, madaline, and backpropagation. Proceedings of the IEEE. 1990;78(9):1415–1442. 10.1109/5.58323
35. Balakrishnama S, Ganapathiraju A. Linear discriminant analysis-a brief tutorial. Institute for Signal and information Processing. 1998;18:1–8.
36. Kramer J, Obejero-Paz CA, Myatt G, Kuryshev YA, Bruening-Wright A, Verducci JS, et al. MICE models: superior to the HERG model in predicting Torsade de Pointes. Scientific reports. 2013;3 10.1038/srep02100
37. https://www.multichannelsystems.com/.
38. Biosystems A. Microelectrode Array (MEA) Axion Biosystems; -. https://www.axionbiosystems.com/products/MEA_Plates_Catalog.
39. Crumb WJ. Loratadine blockade of K+ channels in human heart: comparison with terfenadine under physiological conditions. Journal of Pharmacology and Experimental Therapeutics. 2000;292(1):261–264.
40. Nozaki Y, Honda Y, Watanabe H, Saiki S, Koyabu K, Itoh T, et al. CSAHi study-2: validation of multi-electrode array systems (MEA60/2100) for prediction of drug-induced proarrhythmia using human iPS cell-derived cardiomyocytes: assessment of reference compounds and comparison with non-clinical studies and clinical information. Regulatory Toxicology and Pharmacology. 2017;88:238–251.
41. Hancox JC, McPate MJ, El Harchi A, hong Zhang Y. The hERG potassium channel and hERG screening for drug-induced torsades de pointes. Pharmacology & therapeutics. 2008;119(2):118–132. 10.1016/j.pharmthera.2008.05.009
42. Ma D, Wei H, Zhao Y, Lu J, Li G, Sahib NBE, et al. Modeling type 3 long QT syndrome with cardiomyocytes derived from patient-specific induced pluripotent stem cells. International journal of cardiology. 2013;168(6):5277–5286. 10.1016/j.ijcard.2013.08.015
43. Gualdani R, Tadini-Buoninsegni F, Roselli M, Defrenza I, Contino M, Colabufo NA, et al. Inhibition of hERG potassium channel by the antiarrhythmic agent mexiletine and its metabolite m-hydroxymexiletine. Pharmacology research & perspectives. 2015;3(5). 10.1002/prp2.160
44. Lee K, Tsien R. Mechanism of calcium channel blockade by verapamil, D600, diltiazem and nitrendipine in single dialysed heart cells. Nature. 1983;302(5911):790 10.1038/302790a0
45. Chamberlain BK, Volpe P, Fleischer S. Inhibition of calcium-induced calcium release from purified cardiac sarcoplasmic reticulum vesicles. Journal of Biological Chemistry. 1984;259(12):7547–7553.
46. Ogata N, Nishimura M, Narahashi T. Kinetics of chlorpromazine block of sodium channels in single guinea pig cardiac myocytes. Journal of Pharmacology and Experimental Therapeutics. 1989;248(2):605–613.
47. Lee SY, Kim YJ, Kim KT, Choe H, Jo SH. Blockade of HERG human K+ channels and IKr of guinea-pig cardiomyocytes by the antipsychotic drug clozapine. British journal of pharmacology. 2006;148(4):499–509. 10.1038/sj.bjp.0706744
48. Yatani A, Brown A, Schwartz A. Bepridil block of cardiac calcium and sodium channels. Journal of Pharmacology and Experimental Therapeutics. 1986;237(1):9–17.
49. Busch A, Eigenberger B, Jurkiewicz N, Salata J, Pica A, Suessbrich H, et al. Blockade of HERG channels by the class III antiarrhythmic azimilide: mode of action. British journal of pharmacology. 1998;123(1):23–30. 10.1038/sj.bjp.0701575
50. YAO JA, TSENG GN. Azimilide (NE-10064) Can Prolong or Shorten the Action Potential Duration in Canine Ventricular Myocytes: Dependence on Blockade of K, Ca, and Na Channels. Journal of cardiovascular electrophysiology. 1997;8(2):184–198. 10.1111/j.1540-8167.1997.tb00780.x
51. Ando H, Yoshinaga T, Yamamoto W, Asakura K, Uda T, Taniguchi T, et al. A new paradigm for drug-induced torsadogenic risk assessment using human iPS cell-derived cardiomyocytes. Journal of pharmacological and toxicological methods. 2017;84:111–127. 10.1016/j.vascn.2016.12.003
52. Helms Richard A and Quan David J Textbook of therapeutics: drug and disease management. In: Lippincott Williams & Wilkins

53. Vicente J, Zusterzeel R, Johannesen L, Mason J, Sager P, Patel V, et al. Mechanistic Model-Informed Proarrhythmic Risk Assessment of Drugs: Review of the CiPA Initiative and Design of a Prospective Clinical Validation Study. Clinical Pharmacology & Therapeutics. 2018;103(1):54–66. 10.1002/cpt.896

54. Paci M, Pölönen RP, Cori D, Penttinen K, Aalto-Setälä K, Severi S, et al. Automatic optimization of an *in silico* model of human iPSC derived cardiomyocytes recapitulating calcium handling abnormalities. Frontiers in physiology. 2018;9 10.3389/fphys.2018.00709

Supplementary material

Cost function demonstration: 2 classes

In the perfect case, we have $l_i = \widehat{l_i}$ and $\widehat{p_i} = 1, \forall i$. Then,

$$s_{N_s} = -\frac{1}{N_s}\sum_{i=1}^{N_s}\Big[\frac{N_s}{n_1}\delta_1(\widehat{l_i})\delta_1(l_i) + \frac{N_s}{n_{-1}}\delta_{-1}(\widehat{l_i})\delta_{-1}(l_i)\Big].$$

$$\iff s_{N_s} = -\frac{1}{N_s}\sum_{i=1}^{N_s}\frac{N_s}{n_1}\delta_1(\widehat{l_i})\delta_1(l_i) - \frac{1}{N_s}\sum_{i=1}^{N_s}\frac{N_s}{n_{-1}}\delta_{-1}(\widehat{l_i})\delta_{-1}(l_i).$$

Moreover, we know that $l_i = 1$, n_1 times and $l_i = -1$, n_{-1} times. Finally, we find that the minimum value is $s_{N_s} = -2$. In the worst case, we have $l_i \neq \widehat{l_i}$ and $\widehat{p_i} = 1, \forall i$. Then,

$$s_{N_s} = -\frac{1}{N_s}\sum_{i=1}^{N_s}\Big[-\alpha\frac{N_s}{n_1}\delta_{-1}(\widehat{l_i})\delta_1(l_i) - \frac{N_s}{n_{-1}}\delta_1(\widehat{l_i})\delta_{-1}(l_i)\Big].$$

Moreover, we know that $l_i = 1$, n_1 times and $l_i = -1$, n_{-1} times. Then,

$$s_{N_s} = \frac{1}{N_s}\Big(\alpha\frac{N_s}{n_1}n_1 + \frac{N_s}{n_{-1}}n_{-1}\Big) \implies s_{N_s} = 1 + \alpha.$$

Cost function demonstration: general case

We have the following cost function:

$$s_{N_s} = -\frac{1}{N_s}\sum_{i=1}^{N_s}\widehat{p_i}\left\{\sum_{j=1}^{k}\Big[\frac{N_s}{n_j}\delta_j(\widehat{l_i})\delta_j(l_i) - \frac{N_s}{n_j}\alpha_j\sum_{\substack{m=1\\m\neq j}}^{k}\delta_m(\widehat{l_i})\delta_j(l_i)\Big]\right\}.$$

In the best case, we have $l_i = \widehat{l_i}$ and $\widehat{p_i} = 1, \forall i$. Then,

$$s_{N_s} = -\frac{1}{N_s}\sum_{i=1}^{N_s}\sum_{j=1}^{k}\frac{N_s}{n_j}\delta_j(\widehat{l_i})\delta_j(l_i).$$

We know how many samples are labeled for each class (n_1 for class 1 and n_2 for class 2). Then,

$$s_{N_s} = -\frac{1}{N_s}\Big(\frac{N_s n_1}{n_1} + \frac{N_s n_2}{n_2} + ... + \frac{N_s n_k}{n_k}\Big) \implies s_{N_s} = -k.$$

On the other hand, in the worst case, we have $l_i \neq \widehat{l_i}$ and $\widehat{p_i} = 1, \forall i$. Then,

$$s_{N_s} = -\frac{1}{N_s}\sum_{i=1}^{N_s}\left\{\sum_{j=1}^{k} -\frac{N_s}{n_j}\alpha_j\sum_{\substack{m=1\\m\neq j}}^{k}\delta_m(\widehat{l_i})\delta_j(l_i)\right\}.$$

$$\iff s_{N_s} = \frac{1}{N_s}\sum_{i=1}^{N_s}\sum_{j=1}^{k}\frac{N_s}{n_j}\alpha_j\sum_{\substack{m=1\\m\neq j}}^{k}\delta_m(\widehat{l_i})\delta_j(l_i).$$

For the same reasons concerning the number of labels in each class, we have:

$$s_{N_s} = \frac{1}{N_s}\Big(\frac{N_s}{n_1}\alpha_1 n_1 + \frac{N_s}{n_2}\alpha_2 n_2 + ...\frac{N_s}{n_k}\alpha_k n_k\Big) \implies s_{N_s} = \sum_{j=1}^{k}\alpha_j.$$

Bidomain and electrode model parameters

C_{el}	R_i	R_{el}
$1nF$	$2M\Omega$	$10M\Omega$

Table A. Parameters used for the imperfect electrode model.

A_m	C_m	σ_i	σ_e
$200cm^{-1}$	$1.0\mu Fcm^{-2}$	$5.0nScm^{-2}$	$5.0nScm^{-2}$

Table B. Bidomain equation parameters used for Multichannel Systems MEA device.

A_m	C_m	σ_i	σ_e
$1200cm^{-1}$	$1.0\mu Fcm^{-2}$	$1.2\mu Scm^{-2}$	$1.2\mu Scm^{-2}$

Table C. Bidomain equation parameters used for Axion MEA device with Pluricyte Cardiomyocytes cell line.

Field Potential Biomarkers computation

In this section, the computation of the biomarkers from FP time series is detailed. Let y be a FP signal. We defined as depolarization part (t_1, y_1) from $t = 0$ to $t = 100ms$ and the repolarization part (t_2, y_2) from $t = 100$ to $t = 1200ms$.

DA (Depolarization Amplitude):

Difference between the maximum and minimum value of the FP during the depolarization.

$$DA = max(y_1) - min(y_1). \tag{1}$$

RA (Repolarization Amplitude):

Maximum in absolute value of the repolarization.

$$RA = max(|y_2|). \tag{2}$$

FPD (Field Potential Duration):

Time difference between RA and the maximum in absolute value of the depolarization.

For the depolarization:

$$t_{dep} = t\left[\underset{t}{\text{argmax}}(|y_1(t)|)\right]. \tag{3}$$

For the repolarization:

$$t_{rep} = t\left[\underset{t}{\text{argmax}}(|y_2(t)|)\right]. \tag{4}$$

Then,

$$FPD = t_{rep} - t_{dep}. \tag{5}$$

AUC_r (Area Under Curve of the repolarization wave)

To get the repolarization, y_2 is truncated around $\pm\Delta t$ of t_{rep}. We used $\Delta t = 100$ms. The trapezoidal rule is used to approximate the integral.

$$\text{AUCr} = \left|\int_{t_{rep}-\Delta t}^{t_{rep}+\Delta t} y_2(t)\mathrm{d}t\right|. \tag{6}$$

RC (Repolarization Center)

Offset of the barycenter (with respect to time) of the repolarization wave.

$$\mathrm{RC} = \int_{t_{rep}-\Delta t}^{t_{rep}+\Delta t} t\bar{y}_2(t)\mathrm{d}t - t_{dep}. \tag{7}$$

With $\bar{y}_2(t)$ a rescaling such that it is strictly positive and integrates to 1 on $[t_{rep} - \Delta t, t_{rep} + \Delta t]$.

RW (Repolarization Width)

Standard deviation of the repolarization wave.

$$\mathrm{RW} = \left[\int_{t_{rep}-\Delta t}^{t_{rep}+\Delta t} t^2\bar{y}_2(t)\mathrm{d}t - \left(\int_{t_{rep}-\Delta t}^{t_{rep}+\Delta t} t\bar{y}_2(t)\mathrm{d}t \right)^2 \right]^{1/2}. \tag{8}$$

FPN (FP Notch)

Potential value $4ms$ after t_{dep}. To be less sensitive to noise, the signal is multiplied by a test function $\phi(t_1) = \exp\left[-\frac{(t_1-(t_{dep}+4))^2}{0.04}\right]$.

$$\mathrm{FPN} = \int_{t_1} y_1(t_1)\phi(t_1)\mathrm{d}t_1. \tag{9}$$

Calcium Signals Biomarkers computation

In this section, the computation of the biomarkers from intracellular calcium concentration time series is detailed. Let y be the intracellular calcium concentration signal.

CA (Calcium Amplitude):

Difference between the maximum and minimum value of the signal.

$$CA = max(y) - min(y). \tag{10}$$

DC (Drowsing Calcium):

Corresponding to the resting calcium, computed as the minimum value of the signal.

$$DC = min(y). \tag{11}$$

CDX (Calcium Duration):

Similarly to APD, CDX is the time interval corresponding to $X\%$ repolarization. Let denote by y_1 the signal from $t = 0ms$ to $t = t\left[\underset{t}{\mathrm{argmax}}(|y(t)|)\right] ms$ and y_2 the signal from $t = t\left[\underset{t}{\mathrm{argmax}}(|y(t)|)\right] ms$ to $t = 1200ms$.

For the depolarization:

$$t_{dep} = t\left[\underset{t}{\mathrm{argmin}}(|y_1(t) - \frac{100-X}{100}CA + DC|)\right]. \tag{12}$$

For the repolarization:

$$t_{rep} = t\left[\underset{t}{\mathrm{argmin}}(|y_2(t) - \frac{100-X}{100}CA + DC|)\right]. \tag{13}$$

Then,

$$CDX = t_{rep} - t_{dep}. \tag{14}$$

Index (electrodes median)	Index (electrodes mean)	Index (electrodes max)	Index	Entry name
0	7			DA
1	8			RA
2	9			FPD
3	10			AUC_r
4	11			RC
5	12			RW
6	13			FPN
14	22	30		RA/DA
15	23	31		DA/RA
16	24	32		RA/FPD
17	25	33		FPD/RA
18	26	34		DA/FPD
19	27	35		FPD/DA
20	28	36		RA/RW
21	29	37		RW/RA
			38	CD90
			39	CD75
			40	CD50
			41	CD25
			42	CA
			43	DC
			44	AUC90
			45	AUC75
			46	AUC50
			47	AUC25
48	49			CA*FPD
			50	CA*CD90
			51	CA*CD75
			52	CA*CD50
			53	CA*CD25
54	58			FPD*CD90
55	59			FPD*CD75
56	60			FPD*CD50
57	61			FPD*CD25
			62 to 66 / 38 to 42	K
			67 to 99 / 43 to 157	Wavelets

X: Specific to TdP risk study. X: Specific to channel study.

'able D. Indices and names of the dictionary entries.

drug	Na IC50 (nM)	Ca IC50 (nM)	K IC50 (nM)	EFTPC (nM)
Ajmaline	8200.0	71000.0	1040.0	1500.0
Amiodarone	4800.0	270.0	30.0	0.5
Amitriptyline	20000.0	11600.0	3280.0	41.0
Bepridil*	3700.0	211.0	33.0	33.0
Chlorpromazine*	4300.0	nan	1470.0	38.0
Cibenzoline	7800.0	30000.0	22600.0	976.0
Cisapride*	14700.0	nan	6.5	4.9
Desipramine	1520.0	1709.0	1390.0	108.0
Diltiazem*	9000.0	450.0	17300.0	122.0
Diphenhydramine	41000.0	228000.0	5200.0	34.0
Dofetilide*	300000.0	60000.0	5.0	2.0
Fluvoxamine	39400.0	4900.0	3100.0	377.0
Haloperidol	7000.0	1700.0	27.0	3.6
Imipramine	3600.0	8300.0	3400.0	106.0
Mexiletine*	43000.0	100000.0	50000.0	4129.0
Mibefradil	980.0	156.0	1800.0	12.0
Nifedipine*	37000.0	60.0	275000.0	7.7
Nitrendipine*	36000.0	0.35	10000.0	3.02
Phenytoin	49000.0	103000.0	100000.0	4500.0
Pimozide*	54.0	162.0	20.0	1.0
Prenylamine	2520.0	1240.0	65.0	17.0
Propafenone	1190.0	1800.0	440.0	241.0
Propranolol	2100.0	18000.0	2828.0	26.0
Quetiapine	16900.0	10400.0	5800.0	33.0
Quinidine*	16600.0	15600.0	300.0	924.0
Risperidone*	102000.0	73000.0	150.0	1.81
Sertindole	2300.0	8900.0	14.0	1.59
Tedisamil	20000.0	nan	2500.0	85.0
Terfenadine*	971.0	375.0	8.9	9.0
Thioridazine	1830.0	1300.0	33.0	208.0
Verapamil*	41500.0	100.0	143.0	81.0

Table E. Drugs known as torsadogenic (red) and non-torsadogenic (green) with their IC50 and EFTPC from Mirams *et al.* *: CiPA compound [1].

drug	Na IC50 (nM)	Ca IC50 (nM)	K IC50 (nM)	EFTPC (nM)
Amiodarone	15900.0	1900.0	860.0	0.8
Astemizole*	3000.0	1100.0	4.0	0.3
Bepridil*	2300.0	1000.0	160.0	35.0
Ceftriaxone	555900.0	153800.0	445700.0	23170.0
Chlorpromazine*	3000.0	3400.0	1500.0	38.0
Cilostazol	93700.0	91200.0	13800.0	128.0
Cisapride*	337000.0	11800.0	20.0	3.0
Clozapine*	15100.0	3600.0	2300.0	71.0
Dasatinib	76300.0	81100.0	24500.0	41.0
Diazepam	306400.0	30500.0	53200.0	29.0
Diltiazem*	22400.0	760.0	13200.0	122.0
Disopyramide*	168400.0	1036700.0	14400.0	742.0
Dofetilide*	162100.0	26700.0	30.0	2.0
Donepezil	38500.0	34300.0	700.0	3.0
Droperidol*	22700.0	7600.0	60.0	16.0
Duloxetine	5100.0	2800.0	3800.0	16.0
Flecainide	6200.0	27100.0	1500.0	753.0
Halofantrine	331200.0	1900.0	380.0	172.0
Haloperidol	4300.0	1300.0	40.0	4.0
Ibutilide*	42500.0	62500.0	18.0	140.0
Lamivudine	1571400.0	54200.0	2054000.0	19540.0
Linezolid	2644500.0	105400.0	1147200.0	59110.0
Loratadine*	28900.0	11400.0	6100.0	0.4
Methadone	31800.0	37400.0	3500.0	507.0
Metronidazole	2073200.0	177900.0	1340200.0	187000.0
Mibefradil	5600.0	510.0	1700.0	12.0
Mitoxantrone	93500.0	22500.0	539400.0	225.0
Moxifloxacin	1112000.0	173000.0	86200.0	10960.0
Nifedipine*	88500.0	12.0	44000.0	8.0
Nilotinib	13300.0	17500.0	1000.0	172.0
Nitrendipine*	21600.0	25.0	24600.0	3.0
Paliperidone	109000.0	193900.0	780.0	69.0
Paroxetine	9800.0	3900.0	1900.0	14.0
Pentobarbital	2686000.0	299000.0	1433900.0	5171.0
Phenytoin	72400.0	21900.0	147000.0	4360.0
Pimozide*	1100.0	240.0	40.0	0.5
Piperacillin	2433800.0	1226000.0	3405100.0	1378000.0
Procainamide	746600.0	389500.0	272400.0	54180.0
Quinidine*	14600.0	6400.0	720.0	3237.0
Raltegravir	824200.0	246700.0	782800.0	7000.0
Ribavirin	2997500.0	622500.0	967000.0	27880.0
Risperidone*	43400.0	34200.0	260.0	2.0
Saquinavir	12100.0	1900.0	16900.0	130.0
Sertindole	6900.0	6300.0	33.0	2.0
Sitagliptin	1220800.0	147100.0	174700.0	442.0
Solifenacin	1500.0	4300.0	280.0	3.0
Sotalol*	7013900.0	193300.0	111400.0	14690.0
Sparfloxacin	2555000.0	88800.0	22100.0	1766.0
Sunitinib	16500.0	33400.0	1200.0	13.0
Telbivudine	1095200.0	713900.0	422700.0	19720.0
Terfenadine*	2000.0	930.0	50.0	9.0
Terodiline	7400.0	4800.0	650.0	145.0
Thioridazine	1400.0	3500.0	500.0	980.0
Verapamil*	32500.0	200.0	250.0	88.0
Voriconazole	1550500.0	414200.0	490900.0	7563.0

Table F. Drugs known as torsadogenic (red) and non-torsadogenic (green) with their IC50 and EFTPC from Kramer *et al.* *: CiPA compound [1].

Compound	Concentration 1			Concentration 2			Concentration 3			Concentration 4		
	hERG	Cav1.2	Nav1.5	hERG	Cav1.2	Nav1.5	hERG	Cav1.2	Nav1.5	hERG	Cav1.2	Nav1.5
Loratadine	100	100	100	100	100	100	99.8	99.9	100	99.5	99.7	99.9
Ibutilide	99.4	100	100	94.7	100	100	64.3	100	100	15.3	99.8	99.8
Droperidol	65.4	99.6	99.9	37.5	98.7	99.6	15.9	96.0	98.6	5.7	88.4	95.8
Mexiletine	99.8	99.9	99.7	98.4	99.2	97.4	86.1	92.6	79.2	38.3	55.6	27.5
Dofetilide	99.0	100	100	96.8	100	100	90.4	100	100	75.0	100	100
Diltiazem	99.9	98.7	100	99.2	88.4	99.6	93.0	43.2	95.7	56.9	7.1	69.1
Chlorpromazine	94.0	97.3	96.9	83.3	91.9	90.9	61.2	78.2	76.0	33.3	53.1	50.0
Clozapine	96.0	97.4	99.4	88.4	92.3	98.0	70.8	79.1	94.1	43.4	54.5	83.4
Clarithromycine	99.7	NA	NA	97.1	NA	NA	76.7	NA	NA	24.8	NA	NA
Cisapride	86.2	100	100	66.7	99.9	100	38.8	99.7	100	16.7	99.2	100
Bepridil	94.1	99.0	99.6	61.5	90.9	95.8	13.8	50.0	69.7	1.6	9.1	18.7
Azimilide	NA	NA	NA	NA	NA	NA	NA	NA	NA	NA	NA	NA

Table G. Percentage of activity using a Hill coefficient equals to 1.

Stop criterion based on the success rate variation

Starting from the cost function defined in 12, let's compute the case where all the samples are well classified but with the lowest probability ($\widehat{l_i} = l_i$ and $\widehat{p_i} = \frac{1}{2}, \forall i$):

$$s_{N_s} = -\frac{1}{N_s}\sum_{i=1}^{N_s}\widehat{p_i}\left\{\sum_{j=1}^{k}\left[\frac{N_s}{n_j}\delta_j(\widehat{l_i})\delta_j(l_i) - \frac{N_s}{n_j}\alpha_j\sum_{\substack{m=1\\m\neq j}}^{k}\delta_m(\widehat{l_i})\delta_j(l_i)\right]\right\}. \tag{15}$$

As all samples are well classified with a probability equals to $\frac{1}{2}$, we have:

$$\widetilde{s}_{N_s} = -\frac{1}{N_s}\sum_{i=1}^{N_s}\frac{1}{2}\sum_{j=1}^{k}\delta_j(\widehat{l_i})\delta_j(l_i). \tag{16}$$

We know how many samples are in each class. Then,

$$\widetilde{s}_{N_s} = -\frac{1}{N_s}\Big(\frac{1}{2}\frac{N_s n_1}{n_1} + ... + \frac{1}{2}\frac{N_s n_k}{n_k}\Big). \tag{17}$$

$$\implies \widetilde{s}_{N_s} = -\frac{k}{2}. \tag{18}$$

If now, just 1 sample x is wrongly classified, we have,

$$s_{N_s} = -\frac{1}{N_s}\Big(\frac{1}{2}\frac{N_s n_1}{n_1} + ... + \frac{1}{2}\frac{N_s n_{j-1}}{n_{j-1}} + \frac{1}{2}\frac{N_s (n_j - 1)}{n_j} + \frac{1}{2}\frac{N_s n_{j+1}}{n_{j+1}} + ... + \frac{1}{2}\frac{N_s n_k}{n_k} - \widehat{p_x}\alpha_j\frac{N_s}{n_j}\Big). \tag{19}$$

$$\implies s_{N_s} = -\frac{k}{2} + \frac{1 + 2\widehat{p_x}\alpha_j}{2n_j}. \tag{20}$$

Then, the variation between the two costs is:

$$\Delta = \mid \widetilde{s}_{N_s} - s_{N_s} \mid . \tag{21}$$

$$\implies \Delta = \frac{1 + 2\widehat{p_x}\alpha_j}{2n_j}. \tag{22}$$

The minimum variation which ensures that the classification did not change is described in Equation 23.

$$\Delta_{min} = \min_{j,\widehat{p_x}}\Big(\frac{1 + 2\widehat{p_x}\alpha_j}{2n_j}\Big). \tag{23}$$

Regardless of the class, the minimum is obtained for $\widehat{p_x} = \frac{1}{2}$. Hence,

$$\Delta_{min} = \min_{j}\Big(\frac{1 + \alpha_j}{2n_j}\Big). \tag{24}$$

A criterion to add a new dimension could be:

$$\mid s_{N_s}^{new} - s_{N_s}^{old} \mid < \alpha\Delta_{min}. \tag{25}$$

With $\alpha \in [0, 1]$, a user parameter. If $\alpha = 1$, we are sure that the classification did not change. If $\alpha < 1$, the classification will be the same, but margins will still increase.

As an example, in the TdP classification we have two classes. If we train on the first 76 compounds, 50 of them have a TdP risk and 36 of them do not have a TdP risk. In

the case we want to penalize the false negative rate (drug labeled as no TdP risk instead of TdP risk) with $\alpha = 2$, we finally obtain:

$$(\alpha_j, n_j) = \begin{cases} (1, 50) \text{ if } j = \text{ TdP risk} \\ (2, 36) \text{ if } j = \text{ no TdP risk} \end{cases} . \tag{26}$$

Then, we have $\Delta_{min} = 0.02$. It means that if the difference between the old cost and the new cost is under than 0.02, we are sure that the classification is the same and only probabilities changed.

Concerning the cross-validation part, we made the choice to repeat the k-fold 500 times. B Fig shows us how the cost is impacted by the number of k-fold. We can see that the cost is more stable for a low number of components. Moreover, the cost is under the Δ_{min} threshold for most of the number of k-fold. Under this condition, the number of repeated k-fold has less importance.

Fig B. Impact of the number of repeated k-fold on the cost function in the torsadogenicity classification with the $\boldsymbol{\Delta_{min} = 0.02}$ range.

References

1. Colatsky T, Fermini B, Gintant G, Pierson JB, Sager P, Sekino Y, et al. The comprehensive in vitro proarrhythmia assay (CiPA) initiative-Update on progress. Journal of pharmacological and toxicological methods. 2016;81:15–20.